

*Research Articles: Systems/Circuits*

**Extensive tonotopic mapping across auditory cortex is recapitulated by spectrally-directed attention, and systematically related to cortical myeloarchitecture**

Frederic K. Dick<sup>1,2,3</sup>, Matt I. Lehet<sup>4,5</sup>, Martina F. Callaghan<sup>7</sup>, Tim A. Keller<sup>4,6</sup>, Martin I. Sereno<sup>8</sup> and Lori L. Holt<sup>4,5</sup>

<sup>1</sup>Department of Psychological Sciences, Birkbeck College, University of London, London, WC1E 7HX

<sup>2</sup>Birkbeck-UCL Centre for Neuroimaging, London, WC1H 0AP

<sup>3</sup>Department of Experimental Psychology, University College London, London, WC1H 0AP

<sup>4</sup>Department of Psychology, Carnegie Mellon University, Pittsburgh, PA 15213

<sup>5</sup>Center for the Neural Basis of Cognition, Carnegie Mellon University, Pittsburgh, PA 15213

<sup>6</sup>Scientific Imaging & Brain Research Center, Carnegie Mellon University, Pittsburgh, PA 15213

<sup>7</sup>Wellcome Trust Center for Neuroimaging, Institute of Neurology, University College London, London, WC1N 3BG

<sup>8</sup>Department of Psychology, San Diego State University, San Diego, CA San Diego, CA 92182-4611

DOI: 10.1523/JNEUROSCI.1436-17.2017

Received: 24 May 2017

Revised: 4 October 2017

Accepted: 6 October 2017

Published: 6 November 2017

**Author contributions:** F.D. and L.L.H. designed research; F.D., M.I.L., T.K., and L.L.H. performed research; F.D., M.I.L., and L.L.H. analyzed data; F.D., M.F.C., M.S., and L.L.H. wrote the paper; M.F.C. and M.S. contributed unpublished reagents/analytic tools.

**Conflict of Interest:** The authors declare no competing financial interests.

Research supported by Rothberg Research Award in Human Brain Imaging of Carnegie Mellon University. M.L. was supported by NIH T90DA022761 and T32GM081760. Thanks to Scott Kurdilla and Debbie Viszlay (SIBR) for imaging support, Antoine Lutti and Nikolaus Weiskopf for physics expertise and generosity with porting the MPM protocol to the SIBR Verio, and the developers of FSL, AFNI, and FreeSurfer for their scientific work and software. Finally, we are grateful to Marlene Behrmann, Jenny Bizley, Maria Chait, Tim Griffiths, Jen Linden, Catherine Perrodin, Chris Petkov, Lars Riecke, Sam Schwarzkopf, Jeremy Skipper, Ediz Sohoglu, Adam Tierney, and three anonymous reviewers of a previous version of the manuscript for extremely useful suggestions and feedback. The Wellcome Centre for Human Neuroimaging is supported by core funding from Wellcome [203147/Z/16/Z].

Corresponding Authors: Frederic K. Dick, Birkbeck/UCL Centre for NeuroImaging, 26 Bedford Way, London, WC1H 0AP, UK +44 20 7079 0815, [f.dick@bbk.ac.uk](mailto:f.dick@bbk.ac.uk); Lori L. Holt, Department of Psychology, Baker Hall, Carnegie Mellon University, 5000 Forbes Avenue, Pittsburgh, PA 15213, +1 (412) 268-4964, [loriholt@cmu.edu](mailto:loriholt@cmu.edu)

**Cite as:** J. Neurosci ; 10.1523/JNEUROSCI.1436-17.2017

**Alerts:** Sign up at [www.jneurosci.org/cgi/alerts](http://www.jneurosci.org/cgi/alerts) to receive customized email alerts when the fully formatted version of this article is published.

Accepted manuscripts are peer-reviewed but have not been through the copyediting, formatting, or proofreading process.

Copyright © 2017 Dick et al.

This is an open-access article distributed under the terms of the Creative Commons Attribution 4.0 International license, which permits unrestricted use, distribution and reproduction in any medium provided that the original work is properly attributed.

1           **Extensive tonotopic mapping across auditory cortex is recapitulated by**  
2           **spectrally-directed attention, and systematically related to cortical**  
3           **myeloarchitecture**

4  
5           Frederic K. Dick<sup>1,2,3</sup> (ORCID ID 0000-0002-2933-3912)  
6           Matt I. Lehet<sup>4,5</sup> (ORCID ID 0000-0002-7601-9360)  
7           Martina F. Callaghan<sup>7</sup> (ORCID ID 0000-0003-0374-1659)  
8           Tim A. Keller<sup>4,6</sup> (ORCID ID 0000-0002-2345-8626)  
9           Martin I. Sereno<sup>8</sup> (ORCID ID 0000-0002-7598-7829)  
10          Lori L. Holt<sup>4,5</sup> (ORCID ID 0000-0002-8732-4977)

11  
12          <sup>1</sup> Department of Psychological Sciences, Birkbeck College, University of London, London,  
13          WC1E 7HX

14          <sup>2</sup> Birkbeck-UCL Centre for Neuroimaging, London, WC1H 0AP

15          <sup>3</sup> Department of Experimental Psychology, University College London, London, WC1H 0AP

16          <sup>4</sup> Department of Psychology, Carnegie Mellon University, Pittsburgh, PA 15213

17          <sup>5</sup> Center for the Neural Basis of Cognition, Carnegie Mellon University, Pittsburgh, PA 15213

18          <sup>6</sup> Scientific Imaging & Brain Research Center, Carnegie Mellon University, Pittsburgh, PA 15213

19          <sup>7</sup> Wellcome Trust Center for Neuroimaging, Institute of Neurology, University College London,  
20          London, WC1N 3BG

21          <sup>8</sup> Department of Psychology, San Diego State University, San Diego, CA San Diego, CA 92182-  
22          4611

23  
24          **Corresponding Authors:**

25  
26          Frederic K. Dick, Birkbeck/UCL Centre for Neuroimaging, 26 Bedford Way, London, WC1H  
27          0AP, UK +44 20 7079 0815, f.dick@bbk.ac.uk

28  
29          Lori L. Holt, Department of Psychology, Baker Hall, Carnegie Mellon University, 5000 Forbes  
30          Avenue, Pittsburgh, PA 15213, +1 (412) 268-4964, loriholt@cmu.edu

31  
32          **Abbreviated Title:** Spectrally-directed attention maps in auditory cortex

33          **Number of Pages:** 49

34          **Number of Figures:** 8

35          **Number of Words for Abstract:** 228

36          **Number of Words for Introduction:** 655

37          **Number of Words for Discussion:** 1402

38          **Conflict of Interest:** The authors declare no competing financial interests.

39  
40          **Acknowledgements:** Research supported by Rothberg Research Award in Human Brain  
41          Imaging of Carnegie Mellon University. M.L. was supported by NIH T90DA022761 and  
42          T32GM081760. Thanks to Scott Kurdilla and Debbie Viszlay (SIBR) for imaging support,  
43          Antoine Lutti and Nikolaus Weiskopf for physics expertise and generosity with porting the MPM  
44          protocol to the SIBR Verio, and the developers of FSL, AFNI, and FreeSurfer for their scientific  
45          work and software. Finally, we are grateful to Marlene Behrmann, Jenny Bizley, Maria Chait,  
46          Tim Griffiths, Jen Linden, Catherine Perrodin, Chris Petkov, Lars Riecke, Sam Schwarzkopf,  
47          Jeremy Skipper, Ediz Sohoglu, Adam Tierney, and three anonymous reviewers of a previous  
48          version of the manuscript for extremely useful suggestions and feedback. The Wellcome Centre  
49          for Human Neuroimaging is supported by core funding from Wellcome [203147/Z/16/Z].  
50

51 **Abstract**

52

53 Auditory selective attention is vital in natural soundscapes. But, it is unclear how attentional  
54 focus on the primary dimension of auditory representation - acoustic frequency - might modulate  
55 basic auditory functional topography during active listening. In contrast to visual selective  
56 attention, which is supported by motor-mediated optimization of input across saccades and pupil  
57 dilation, the primate auditory system has fewer means of differentially sampling the world. This  
58 makes spectrally-directed endogenous attention a particularly crucial aspect of auditory  
59 attention. Using a novel functional paradigm combined with quantitative MRI, we establish in  
60 male and female listeners that human frequency-band-selective attention drives activation in  
61 both myeloarchitecturally-estimated auditory core, and across the majority of tonotopically-  
62 mapped non-primary auditory cortex. The attentionally-driven best-frequency maps show strong  
63 concordance with sensory-driven maps in the same subjects across much of the temporal  
64 plane, with poor concordance in areas outside traditional auditory cortex. There is significantly  
65 greater activation across most of auditory cortex when best frequency is attended, versus  
66 ignored; the same regions do not show this enhancement when attending to the least-preferred  
67 frequency band. Finally, the results demonstrate that there is spatial correspondence between  
68 the degree of myelination and the strength of the tonotopic signal across a number of regions in  
69 auditory cortex. Strong frequency preferences across tonotopically-mapped auditory cortex  
70 spatially correlate with  $R_1$ -estimated myeloarchitecture, indicating shared functional and  
71 anatomical organization that may underlie intrinsic auditory regionalization.

72

73

74

75

76

77 **Significance**

78

79 Perception is an active process especially sensitive to attentional state. Listeners direct auditory  
80 attention to track a violin's melody within an ensemble performance, or to follow a voice in a  
81 crowded cafe. Although diverse pathologies reduce quality of life by impacting such spectrally-  
82 directed auditory attention, its neurobiological bases are unclear. We demonstrate that human  
83 primary and non-primary auditory cortical activation is modulated by spectrally-directed attention  
84 in a manner that recapitulates its tonotopic sensory organization. Further, the graded activation  
85 profiles evoked by single frequency bands are correlated with attentionally-driven activation  
86 when these bands are presented in complex soundscapes. Finally, we observe a strong  
87 concordance in the degree of cortical myelination and the strength of tonotopic activation across  
88 several auditory cortical regions.

89

90 **Introduction**

91

92 Listeners shift attention across multiple simultaneously-present acoustic dimensions to home in  
93 on those that are diagnostic in guiding behavior (Idemaru and Holt, 2011; Herrmann and Henry,  
94 2013; Shamma and Fritz, 2014). In nonhuman animal studies task-based spectral attention  
95 adaptively modulates auditory neurons' spectrotemporal response fields (Fritz et al., 2010).  
96 Human neuroimaging results reveal that attention to streams of high- versus low-frequency  
97 acoustic input can modulate activity in tonotopically-defined regions (Paltoglou et al., 2009), as  
98 can imagery of higher versus lower frequencies (Oh et al., 2013). In and directly around  
99 Heschl's gyrus, there are strong frequency-band-specific attentional effects to high and low  
100 pure-tone streams presented to opposite ears (Da Costa et al., 2013) and a shared topography  
101 of sensory and attentionally-driven responses (Riecke et al., 2016). These results establish that  
102 endogenous attention directed across acoustic frequency, the primary axis of auditory  
103 representation, can modulate human cortical activity in a tonotopic manner around Heschl's  
104 gyrus. But, there remain important unanswered questions about the neurobiological basis of  
105 human spectrally-directed attention.

106 First, does the topography of attention to different frequency bands recapitulate tonotopic  
107 organization in human primary auditory cortex? Non-human animal physiology establishes  
108 spectrally-directed attention in myelo- and cyto-architectonically-defined primary areas in  
109 'auditory core' (Fritz et al., 2007b; Shamma and Fritz, 2014). However, although two recent  
110 neuroimaging studies have shown strong similarities between stimulus- and attentionally-driven  
111 tonotopic organization in and directly around Heschl's gyrus (Da Costa et al., 2013; Riecke et  
112 al., 2016), it has not yet been possible to unambiguously localize this effect to human auditory  
113 core. Here, we use high-resolution quantitative MRI (Pierpaoli, 2010) to estimate myelo-

114 architectonically-defined auditory core, and demonstrate that spectrally-directed attention  
115 modulates its activation in a tonotopically-organized manner.

116 Second, is attentionally-driven tonotopic organization present outside of auditory core? In  
117 humans, Riecke et al. (2016) found no significant evidence for tonotopically organized effects of  
118 spectral attention outside of early auditory areas, but did show that the information content of  
119 non-primary cortical frequency representations was sufficient for above-chance decoding of  
120 listeners' frequency-selective attentional focus. The lack of attentionally-driven tonotopic maps  
121 contrasts with the finding that most non-primary cortical visual areas exhibit strong  
122 retinotopically-specific attentional effects (Saygin and Sereno, 2008). Using intensive data  
123 collection (>7000 functional volumes per subject) we present evidence for widespread,  
124 tonotopically-organized modulation by spectral attention across much of auditory cortex, with  
125 individual differences in individual participants' tonotopic maps reproduced in attentionally-  
126 driven maps.

127 Third, what is the effect of frequency-selective attention being directed to a voxel's non-  
128 preferred frequency band? Detailed fMRI studies of stimulus-driven frequency response  
129 functions (Schönwiesner and Zatorre, 2009; Moerel et al., 2013) have shown graded and multi-  
130 peaked frequency responses across human auditory cortex. However, it is unclear whether  
131 these more complex patterns are recapitulated by attention to a given frequency band. In the  
132 context of three distinct frequency bands, (Riecke et al., 2016) found that attentional filters  
133 appeared to be bandpass in and around Heschl's gyrus. Here, using a five-frequency-band  
134 paradigm, we establish that graded response profiles evoked by single frequency bands are  
135 strongly associated with attentionally-driven response profiles to those frequencies across much  
136 of auditory cortex. We also show that a systematic topography of 'dis-preferred' frequency can  
137 be driven by attention, and establish the regionalization of spectral attentional effects relative to  
138 prior studies of crossmodal auditory attention (Petkov et al., 2004).

139 Finally, is there spatial correspondence between auditory cortical anatomy, as measured by the  
140 local change in  $R_1$ -estimated myelination, and fMRI-assessed strength of relative frequency  
141 selectivity? Post-mortem Gallyas staining to establish human myeloarchitecture reveals  
142 considerable variability in auditory cortical myelination that is associated with MRI signal change  
143 in the same brain (Wallace et al., 2016). Likewise, variation in cortical myelination estimated  
144 using T1-weighted/T2-weighted ratio approaches also appears to correspond spatially with  
145 some functional variation in the superior temporal lobe (Glasser et al., 2016). Here, we  
146 demonstrate that there is spatial concordance between the degree of myelination and the  
147 amplitude of the frequency-selective tonotopic signal across several regions in auditory cortex.

## 148 **Methods**

149

150 **Experiment Overview.** We used a novel paradigm in which listeners direct attention to a series  
151 of four-tone ‘mini-sequences’ that fall within one of five possible spectral bands, without any  
152 spatial cues. The task is to monitor for temporally-adjacent mini-sequence repeats within the  
153 attended band. Inasmuch as this places a very high demand on encoding and integrating  
154 spectral sequences within a delimited frequency range, we expect it to be especially effective in  
155 evoking strong responses in non-primary auditory cortical areas. The goal is to address where,  
156 specifically, in the auditory system spectral gain from attention is evident, and akin to long-  
157 standing work in vision (Kastner and Ungerleider, 2000), to delineate the topographic maps  
158 across which attentional modulation is apparent.

159

160 The target mini-sequences were embedded in either an informationally-sparse or  
161 informationally-dense acoustic scene (Figure (Fig.) 1). Streams of four-tone mini-sequences  
162 were presented in either a single band (‘tonotopy’, Fig. 1a), or accompanied by mini-sequences  
163 in a ‘distractor’ frequency band, the center frequency of which varied in the frequency distance



164 from the attended band across blocks ('attention-tonotopy', abbreviated 'attn-tono', Fig. 1b). A  
165 verbal cue directed listeners' attention to a specific frequency band, within which listeners  
166 monitored four-tone mini-sequences for repeats; the 'distractor' band in attn-tono blocks also  
167 contained repeats. Using a discretized version of a phase-encoded fMRI design (Serenio et al.,  
168 1995; Schwarzkopf et al., 2011; Rao and Talavage, 2005; Herdener et al., 2013; Langers et al.,  
169 2014), the cued frequency band stepped up or down in orderly steps across the acoustic  
170 spectrum across a 64-sec cycle [Fig. 1c]. Phase-encoded tonotopic designs benefit from the  
171 power and robustness of the 'travelling wave' method for topographic cortical mapping of  
172 smoothly varying representations (Engel, 2012); the discretized (blocked) version we use here  
173 allows use of the verbal cue, and has the advantage of being able to be analyzed using both  
174 Fourier and regression approaches. This allowed us to include an additional, 'randomized' attn-  
175 tono condition that contributed both as a control condition in Fourier analyses, and also as an  
176 additional attn-tono run in regression analyses (see Fig. 1d). The tone stimuli from this condition  
177 were *identical* to the 'stepped' attn-tono condition, but the order of the verbal cues directing  
178 listeners' attention to a specific frequency band was scrambled in their assignment to blocks.  
179 This preserved the acoustics across conditions, but eliminated the consistent 'stepping' of  
180 attention through the frequency spectrum in the randomized condition thereby destroying the  
181 consistent phase-lag associated with specific frequency bands that support Fourier analyses  
182 [schematized in Fig. 1e, and see below]. Thus, to the extent that there are attentionally-driven  
183 frequency-selective maps in auditory cortex we expect tonotopically-organized attentional maps  
184 to be apparent in the 'stepped,' but not the 'randomized' attn-tono conditions under Fourier  
185 analyses. In contrast, regression analyses include a model of attention, allowing 'stepped' and  
186 'randomized' attn-tono conditions to be pooled to investigate the impact of attention on cortical  
187 activation. Across both Fourier and regression analyses, the 'stepped' attn-tono conditions were  
188 collapsed across runs for which the cued frequency band stepped up in frequency and those



189 that stepped down; inclusion of each simply balanced the directional movement of attention  
190 through the acoustic spectrum across the experiment.

191

192 In summary, in the *attn-tono* conditions, attention alone was available to differentially drive  
193 responses to an approximately constant acoustic input, whereas in the *tonotopy* condition,  
194 responses were driven by spectrally-selective stimuli as well as by attention.

195

196 We analyzed mapping data using Fourier methods with individual and surface-based group  
197 analysis methods, as described previously (Sereno et al., 1995; Hagler et al., 2006; 2007). With  
198 this approach, voxels preferentially responding to a certain phase in a 'stepped' stimulus cycle  
199 are defined as those that have a significantly higher signal amplitude at this stimulus temporal  
200 frequency (meaning the slow frequency of the repeat of the spectral ramp) than at the average  
201 of other 'noise' frequencies (see Fig. 1e). Significant signal *phases* (a particular position in the  
202 cycle) are then mapped to a color scale to indicate the voxel's 'best frequency' and signal  
203 amplitude is mapped to the voxel's color saturation (Fig. 1f). We time-reversed runs stepping  
204 down in frequency and averaged them with runs stepping up in frequency (Sereno et al., 1995;  
205 Talavage et al., 2004; Dick et al., 2012; Ahveninen et al., 2016). Cross-subject averaging of  
206 phase-encoded mapping data was performed using a method described previously (Hagler et  
207 al., 2007) in which the real and imaginary components of the signal with respect to the stepped  
208 cycle were sampled to the cortical surface and then averaged across subjects, preserving any  
209 phase information that was coherent over subjects.

210

211 Using previously established methods (Dick et al., 2012; Sereno et al., 2013; Lutti et al., 2014)  
212 see also (Glasser et al., 2016), we used high-resolution quantitative multi-parameter mapping to  
213 generate maps of estimated cortical myelination based on longitudinal relaxation times  
214 (quantitative  $T_1$ ). Recent work by multiple labs supports the hypothesis that  $T_1$  relaxation is

215 reliably associated with quantitative differences in myelination in white matter and cortex  
216 (Serenio et al., 2013; Callaghan et al., 2014; Stüber et al., 2014; Dinse et al., 2015; Tardif et al.,  
217 2015; Turner, 2015; Tardif et al., 2016). Here, we calculated each subject's  $R_1$  ( $1/T_1$ ) values,  
218 where the greater the  $R_1$ , the higher the inferred myelin content. These  $R_1$  values were  
219 resampled onto his or her surface at a cortical depth fraction of 0.5, and also averaged across  
220 individuals using sulcus-aligned cortical-surface-based procedures (see below for further  
221 details).

222

223 **Participants.** Eight adults (aged 23-45 y, mean 28 y; 6 female) participated; none reported a  
224 history of neurological disease or communication disorders. All had some childhood and/or adult  
225 musical training (one had a music degree), and had previous experience with longer scanning  
226 sessions. While musical training seemed to facilitate learning the experimental task, subsequent  
227 behavioral studies in the lab have shown that musically-naive subjects can also attain excellent  
228 performance with similar levels of training on this and even more demanding related tasks.

229

230 **Stimuli and Design.** Stimuli were created using custom code in Matlab version 2015a  
231 (Mathworks, Inc.) and SoX version 14.4.2 (sourceforge.net). The basic stimulus unit was a four-  
232 tone *mini-sequence* (140 ms sine-wave tones including 10 ms linear amplitude ramp), with each  
233 tone drawn with replacement from a seven-semitone, band-delimited pool centered around one  
234 of five frequencies (300, 566, 1068, 2016, 3805 Hz; Fig. 1a). Fourteen mini-sequences formed a  
235 *block* (mean inter-sequence silent interval 240 ms, SD 10 ms). Each block contained one to  
236 three mini-sequence repeats (1:2:1 ratio of 1, 2, and 3 repeats). When there was more than one  
237 repeat per block, mini-sequence repeat pairs were separated by at least one intervening mini-  
238 sequence. Each block began with a verbal prompt: '*hear*', '*high*', or '*low*'; loudness-equalized  
239 Mac 'Victoria' voice, mean duration 506 ms (SD 36 ms), padded with silence to 800 ms total

240 duration. This prompt was followed by 800 ms silent gap (tonotopy) or tone-cue (attn-*tono*), then  
241 the 14 mini-sequences (11.2s in total), for a total block duration of 12.8s.

242

243 The task was to detect mini-sequence repeats in the attended frequency band (i.e., a 1-back  
244 task). In the tonotopy condition, mini-sequences were confined to a single frequency band  
245 preceded by the neutral verbal prompt '*hear*' (Fig. 1a). In two of the four single-band tonotopy  
246 runs, block center frequency was stepped from low-to-high over a 64-second cycle with 8  
247 cycles/run; step direction was reversed (high-to-low) for the other two runs. This is a 'discrete'  
248 version of phase-encoded designs commonly used in visual, somatosensory, and auditory  
249 mapping studies (Engel et al., 1994; Sereno et al., 1995; Da Costa et al., 2011; Dick et al.,  
250 2012; Langers and van Dijk, 2012; Langers et al., 2014; Saenz and Langers, 2014).

251

252 The *attn-*tono** condition had the exact mini-sequence patterns from the tonotopy blocks, but  
253 there also were simultaneous, competing mini-sequences in a distinct frequency band with a  
254 center frequency at least 14 semitones apart (Fig. 1b; 300 vs. 1068 Hz; 300 vs. 2016 Hz; 300  
255 vs. 3805 Hz; 566 vs. 2016 Hz; 566 vs. 3805 Hz; 1068 vs. 3805 Hz; not all center frequencies  
256 were paired due to the 14-semitone constraint). The verbal prompt (*high* or *low*) initiating each  
257 *attn-*tono** block signaled participants to perform the 1-back task on either the higher or lower  
258 frequency band. Immediately after the verbal prompt, a randomly-ordered pair of sine-wave  
259 tones cued the center frequencies of the upcoming block (140 ms tones including 8 ms linear  
260 on/off amplitude ramp; 26 ms inter-tone silence, tone pair followed by 494 ms silence, total  
261 duration 800 ms). Crucially, there were mini-sequence repeats even in the unattended band to  
262 assure that attention directed to the task was endogenously driven rather than being attracted  
263 by stimulus repetition effects (Barascud et al., 2016).

264

265 There were two attn-tono conditions: 'stepped' and 'randomized'. Analogous to single-band  
266 tonotopy runs, in stepped attn-tono runs the verbally-cued frequency band implicitly stepped up  
267 (2 runs) or down (2 runs) in frequency over a 64-sec *cycle* (Fig. 1c). This cued iterative stepping  
268 through the frequency spectrum facilitates transfer of attention to each frequency band (as in  
269 traditional phase-encoded designs) and supports Fourier approaches to analysis (Fig. 1e). Each  
270 randomized attn-tono run was acoustically identical to a stepped run, but the verbal prompt was  
271 manipulated so that there was no systematic, stepped organization of mini-sequence center  
272 frequencies through the spectrum (Fig. 1d). For this condition, frequency bands were cued at  
273 inconsistent phase lags within the 8 cycles/run, thereby phase-canceling any periodic attentional  
274 response; this is schematized in Fig 1e. This randomized-order control is important, as there is  
275 a small (~1 octave) overall shift in spectral mean over the course of an attn-tono stimulus cycle  
276 that is unavoidable due to the constraints on the pairing of frequency bands.

277

278 Each of the twelve 9.6-minute-long runs was composed of eight 64s cycles plus 32-sec silent  
279 periods at the beginning and end of each run to allow for calculation of baseline auditory  
280 activation (Klein et al., 2014).

281

282 **Behavioral Thresholds and Training.** Participants first underwent behavioral tests of monaural  
283 pure-tone thresholds and binaural thresholds for detecting mini-sequences in quiet and in  
284 acoustic noise generated by the MRI scanner running the multiband EPI sequence. This  
285 provided a basis for adjusting center frequency amplitudes to approximate equal loudness in  
286 scanner noise. Participants also trained on the mini-sequence detection task in quiet and in  
287 acoustic scanner noise across two sessions.

288

289 **Imaging Data Acquisition.** Structural and functional images were acquired on a 3-Tesla  
290 Siemens Verio wide-bore MRI scanner at the Scientific Imaging and Brain Research (SIBR)

291 Center at Carnegie Mellon University using a phased array 32-channel head coil across three  
292 scan sessions on separate days. Stimulus presentation was under the control of a MacPro  
293 running PsychToolbox 3.0.12 in Matlab (The Mathworks, Inc.), with audio output to an external  
294 AD/DA converter (Babyface, RME) connected to an amplifier (Pylepro) that delivered stimuli to  
295 participants in the scanner diotically over MRI-compatible earbuds (Sensimetrics S14). All  
296 stimuli were pre-filtered to equalize sound stimuli according to the earbuds' frequency response.  
297 After participants were settled into the bore, sound volume was adjusted so that participants  
298 could comfortably hear all frequencies through scanner noise. Participants wore a fiber optic  
299 response glove (Current Designs) that communicated with a Brain Logics I/O device  
300 (Psychology Software Tools, Inc); participants used the glove to respond to mini-sequence  
301 repeats using the right index finger. During all functional scans, subjects closed their eyes to  
302 reduce the potential for stimulus-correlated eye movements.

303

304 In the initial scanning session (~50 min), we acquired multi-parameter mapping (MPM) images  
305 for quantitative myelin mapping and structural identification of primary auditory cortex on an  
306 individual basis while participants watched a film. Proton density-weighted (PDw), T1-weighted  
307 (T1w), and magnetization transfer (MTw) images were acquired using an in-house 3D FLASH  
308 pulse sequence (voxel size:  $0.8 \times 0.8 \times 0.8 \text{ mm}^3$ , matrix =  $320 \times 280 \times 208$ , TR = 25.0 ms,  
309 bandwidth 488 Hz/px, excitation flip angle:  $6^\circ$  (PDw/MTw) or  $21^\circ$  (T1w), slab rotation  $30^\circ$ ). To  
310 accelerate this high resolution acquisition, a partial Fourier acquisition (6/8 coverage) was used  
311 in the inner phase-encoded direction (RL) and parallel imaging was used along the outer phase  
312 encoding direction (AP), reconstructed using the GRAPPA algorithm (acceleration factor 2, 18  
313 integrated auto-calibration lines) as implemented on the scanner platform. Four gradient echoes  
314 were acquired for each contrast (TE=2.5, 4.74, 6.98, 9.22 ms) after each excitation pulse and  
315 averaged to improve SNR (Helms et al., 2009). Each FLASH acquisition lasted 9 minutes 45  
316 seconds. Quantitative  $R_1$  ( $=1/T1$ ) maps were estimated from the PDw and T1w images

317 according to the model developed by Helms et al. (Helms et al., 2008) including a correction for  
318 RF transmit field inhomogeneities (Lutti et al., 2010) and imperfect spoiling (Preibisch and  
319 Deichmann, 2009). The transmit field map was calculated using a 3D EPI spin-echo  
320 (SE)/stimulated echo (STE) method (Lutti et al., 2010; 2012); FOV = 256 x 192 x 192 mm,  
321 matrix = 64 x 64 x 48, TE = 53.14 ms, TM = 47.60 ms, TR = 500 ms, bandwidth = 2298, nominal  
322  $\alpha$  varying from 135° to 65° in steps of 5°, acquisition time 6 minutes) and was corrected for off-  
323 resonance effects using a standard B0 field map (double gradient echo FLASH, 3x3x2 mm  
324 isotropic resolution, whole-brain coverage).

325

326 The final two scanning sessions acquired functional data for four runs each of the tonotopy,  
327 'stepped' attn-tono, and 'randomized' attn-tono conditions. The runs were interleaved across  
328 conditions and designed to assess phase-encoded functional influences of selective attention  
329 across frequency ('stepped' attn-tono), the functional response to identical acoustics without  
330 systematic phase encoded shifts of attention ('randomized' attn-tono), and functional responses  
331 to single frequency bands identical to the attended bands in attn-tono, with phase-encoded  
332 steps through frequency and no distractor frequency bands (tonotopy). Across all functional  
333 runs, participants engaged in detecting repeats (1-back) of the four-tone mini-sequences. Run  
334 order was counterbalanced according to condition and whether the cycle involved steps up or  
335 down in frequency.

336

337 Functional images were acquired using a T2\*-weighted echo-planar imaging (EPI) pulse  
338 sequence (44 oblique axial slices, in plane resolution 3 mm x 3 mm, 3 mm slice thickness, no  
339 gap, repetition time TR = 1000 ms, echo time TE = 41 ms, flip angle = 61°, matrix size = 64 x  
340 64, field of view FOV = 192 mm). All EPI functional scans were performed using 4x multi-band  
341 acceleration (Feinberg et al., 2010; Feinberg and Setsompop, 2013). There were 584 repetitions

342 acquired per run, with the first 8 images discarded to allow for longitudinal magnetization to  
343 arrive at equilibrium. Runs were pseudo-randomly ordered across participants.

344

345 **Image Preprocessing.** *Cortical surface creation, and mapping of  $R_1$  values.* Each subject's  
346 cortical surface was reconstructed from a contrast-optimized synthetic FLASH volume, created  
347 with `mri_synthesize` in Freesurfer from scaled and truncated versions of the T1 and proton-  
348 density volumes; another MPRAGE-like synthetic image was created for use with the automated  
349 Freesurfer Talairach procedure. Both volumes were conformed to 1mm isotropic resolution and  
350 used in a customized reconstruction pipeline version. (In particular, the subject's PD volume  
351 was used to deskull the synthetic FLASH image using a 'shrink-wrap' technique (Dale and  
352 Sereno, 1993). After inspection for reconstruction quality,  $R_1$  values were resampled from 50%  
353 cortical depth fraction to the subject's surface, and also morphed to the unit icosahedron for  
354 cross-subject curvature-aligned cortical surface based averaging (Fischl et al., 1999).

355

356 *EPI processing.* Each functional image from both sessions was aligned to a reference volume  
357 from the middle of the first run using AFNI's `3dvolreg`; registration and motion correction  
358 goodness were hand-checked for each run. The reference volume was aligned to the subject's  
359 cortical surface using boundary-based registration in Freesurfer (Greve and Fischl, 2009),  
360 verified using manual blink comparison, and applied to the volume-aligned EPI data for  
361 resampling. EPI data were analyzed in native space without any spatial smoothing using both  
362 Fourier and general linear methods.

363

364 **Experimental Design and Statistical Analysis.** As noted above, the fMRI experiment used a  
365 'discrete' version of a traditional phase-encoded design, such that both Fourier-based and  
366 general linear model approaches could be used. Fourier analyses were carried out in `csurf`  
367 (<http://www.cogsci.ucsd.edu/~sereno/.tmp/dist/csurf>) with individual and group analysis methods



368 employed as previously described (Sereno et al., 1995; Sereno and Huang, 2006; Hagler et al.,  
369 2007). Functional activation amplitude was estimated as the Fourier amplitude of the periodic  
370 BOLD signal (proportional to percent response) at the frequency of the stimulus cycle (8  
371 repetitions per run). An F statistic was calculated by comparing that amplitude to the average  
372 amplitude of other 'noise' frequencies (Hagler et al., 2007). Periodic signal components with  
373 very low frequencies (due to slow head motion) and the second and third harmonic of the  
374 stimulus were excluded as neither signal nor noise (this is mathematically equivalent to first  
375 linearly regressing out these frequencies as nuisance variables before calculating significance).  
376 The phase of the signal, which corresponds to a particular point of the stimulus cycle, was then  
377 mapped to a color scale and the amplitude of the signal at each vertex was mapped to color  
378 saturation (Gouraud sharing within each face). Runs with downward frequency steps were time-  
379 reversed and averaged with upward-stepped scans in order to cancel fixed voxel-specific delays  
380 in the BOLD response.

381

382 Linear modeling was carried out in FSL (Smith et al., 2004). For all runs, the motion-registered  
383 data were high-pass-filtered (100 sec) and prewhitened; a hemodynamic model corresponding  
384 to each stimulated and attended (tonotopy condition) or attended (stepped, randomized attn-  
385 tono conditions) frequency band was created by convolving the 12.8-sec block with a gamma  
386 function (lag 6s, SD sc). In a separate multiple regression, the unattended (ignored) frequency  
387 band was modeled for both stepped and randomized attn-tono conditions. The verbal cue was  
388 also modeled; all models were temporally filtered before multiple regression. Coefficients from  
389 the first-level contrasts for each of the four runs were combined in a fixed-effects analysis for  
390 each condition; data from the stepped and random block conditions were also combined in an  
391 eight-run average.

392

393 Cross-subject averaging of phase-encoded mapping data was performed using the  
394 methodology developed by Hagler and Sereno (2006) in which the real and imaginary  
395 components of the signal with respect to the stimulus ramp are averaged across subjects,  
396 preserving any phase information consistent between subjects. This was performed by  
397 projecting each participant's phase-encoded map to the FreeSurfer spherical atlas using  
398 `mri_surf2surf`, performing 1 step of surface-based smoothing ( $< 1$  mm FWHM in 2D), averaging  
399 across subjects at each vertex, then painting back onto a single subject's surface for viewing.  
400 For the multiple regression analyses, the same sampling process was used to sample each  
401 subject's contrast parameter estimates for cross-subject averaging and t-tests.

402

403 Surface-based cluster exclusion was used to correct for multiple comparisons in the group-wise  
404 averages (`surfclust` and `randsurfclust` from (Hagler et al., 2006)). The exclusion criterion (only  
405 surface clusters  $> 78$  mm<sup>2</sup> unless otherwise noted) was determined based on the minimum  
406 estimated cortical area from iterative random sampling of cluster sizes (N=10000 iterations per  
407 hemisphere in `randsurfclust`) required to achieve a corrected alpha of  $p < 0.001$  for each  
408 hemisphere, based on an initial uncorrected alpha of vertex-wise  $p < 0.01$ .

409

410 As an alternative means of defining primary auditory cortex, we projected the Morosan et al.  
411 (2001) 3D raw probability maps provided in the AFNI (version 16.3.13, Cox, 2012) to a  
412 FreeSurfer "fsaverage" brain registered to the Talairach target brain, resampled the data onto  
413 the cortical surface, and thresholded at  $p > 0.30$  to create ROI labels. The labels were  $\sim 2$  mm  
414 FWHM (five steps) surface-smoothed with manual removal of isolated marked vertices (due to  
415 "spillover" from the 3D to 2D projection within the lateral fissure), then spherically morphed to  
416 each subject. The labels were individually inspected (and filled if there were small holes in the  
417 label), then a boundary was delineated around each label on each subject's flattened auditory  
418 cortical patch.

419

420 *ROI analyses.* We quantified the similarity between frequency band response profiles driven by  
421 stimulus+attention (tonotopy) versus attention alone (attn-tono) in a 'quilt' of small cortical-  
422 surface-based ROIs that tiled the temporal plane. ROIs (as seen in Fig. 5b) were created on a  
423 single subject's right and left hemisphere flattened patches by flooding all vertices within a 4mm  
424 radius around a central selected vertex. Each of the ROIs (57 in the right hemisphere patch, and  
425 68 in the slightly larger left patch) were then spherically morphed to the other 7 subjects'  
426 flattened patches. Spurious ROI sampling on the edges of the patches was manually corrected  
427 on the original subject's inflated surface and re-morphed to all other subjects. Each ROI was  
428 then projected into the registered native-space EPI volume using Freesurfer's `mri_label2vol`  
429 (sampled from the grey-white boundary to 0.8 of the calculated cortical depth, with `fillthresh` set  
430 to 0.5). For each subject, within each ROI, we calculated the average parameter estimate for  
431 each frequency band for tonotopy, and combined stepped and randomized attn-tono conditions.  
432 For each ROI, we then ran a linear model with average tonotopy parameter estimates for the 5  
433 frequency bands predicting average attn-tono parameter estimates for the same bands,  
434 including subjects as a random factor. The resulting partial t-statistic for each ROI was z-  
435 transformed and color-rendered in Fig. 5b, with p-value thresholds Bonferroni-corrected to  $p <$   
436 0.05 for the number of ROIs per hemisphere, and indicated by the white outline surrounding the  
437 set of ROIs that surpass this z-threshold.

438

439

## Results

440

### *Fourier-based Analyses*

442

443 *Stimulus- and attentionally-driven tonotopic organization in human auditory core.* As a  
444 necessary first step, we characterized basic tonotopic (stimulus-driven) organization in and

445 immediately around myelin-estimated auditory core. The group-average  $R_1$ -based estimates of  
446 myelination (inflated hemispheres in left-most panel of Fig. 2) show that the highest  $R_1$  values  
447 occur within primary somatomotor areas along the central sulcus, and in the typically keyhole-  
448 shaped presumptive 'auditory core' lying along and immediately surrounding Heschl's gyrus. It  
449 is important to note that myelination varies within auditory core and that the lateral and medial  
450 borders are less sharply demarcated (reviewed in Hackett et al., 2001, and Dick et al., 2012). To  
451 show this variation, we plot isointensity  $R_1$  contours in the cortical flat patches in Figs 2a-c (with  
452 the curvature-based boundaries of Heschl's gyrus overlaid in dotted lines). To help identify the  
453 discontinuities in  $R_1$  that would correspond to the putative borders of auditory core, we  
454 calculated the  $R_1$  gradient along the surface (Glasser et al., 2016). Lines drawn along the peak  
455 gradient amplitude (not shown) corresponded well with the outermost  $R_1$  isointensity contour in  
456 Fig. 2 ( $0.66 \text{ s}^{-1}$ ). (It is important to note the gradient at the lateral edge of presumptive core is  
457 quite shallow, and - as in postmortem myelin stains - it is therefore more difficult to establish an  
458 unambiguous lateral border, as could be surmised from the greater lateral spread of the  
459 isointensity contours. The shape and size ( $\sim 1.2\text{cm} \times 2.4\text{cm}$ ) of presumptive auditory core in this  
460 sample also agreed with the results from Dick et al. (2012) at the same  $R_1$  threshold (with the  
461 latter average core slightly narrower, not shown here).

462

463 The group-averaged topography of preferred frequency around auditory core has a typical  
464 arrangement (Dick et al., 2012; De Martino et al., 2015b), with the core surrounded by a high-  
465 frequency 'V'. Preferred frequency descends into the center of core (where  $R_1$  values are  
466 highest) before reversing and slowly ascending to mid-frequency preferred frequencies  
467 anterolaterally (and to some extent posterolaterally). Fig. 3 shows tonotopic maps for each  
468 individual listener. In general, the relationship between auditory core and tonotopy group is  
469 conserved across listeners, but with some variability in the shape and extent of the isointensity  
470  $R_1$  contours. In particular, S2, S6 (right hemisphere), S7, and S8 (right hemisphere) had

471 irregularly shaped and 'blotchy' isointensity contours. While there is a fair degree of individual  
472 variability in results from human postmortem cyto- and myelo-architectonic studies of auditory  
473 core and surrounding areas (Hackett et al., 2001; Sweet et al., 2005), this was somewhat  
474 greater than expected variation given other work in our laboratory (Dick et al., 2012; Lutti et al.,  
475 2014; Carey et al., 2017). As an independent estimate of primary auditory areas, we also  
476 morphed the Morosan et al. (2001) 3D probabilistic map of primary auditory areas (TE1.0) using  
477 previously established methods (see Methods); the outlines of the morphed labels  
478 corresponding to  $p > 0.30$  of being within TE1.0 are overlaid in black dotted lines in Figure 3.

479

480 We then asked whether 'attention-tonotopic' mapping resembled the tonotopic case in and  
481 around auditory core. Here, the group-level spatial distribution of tonotopy is closely  
482 recapitulated when spectrally-directed attention ('stepped' attn-ono condition) alone modulates  
483 activation (Fig. 2b). This holds true in and around the keyhole-shaped hyperintensity defining  
484 core, with a slight exception in the transition from higher to lower frequency preference in mid  
485 core. In contrast (and as expected) the group-level attn-ono response for the randomized  
486 control condition is much weaker (Fig. 2c), with almost no correspondence with the tonotopic  
487 map, despite being acoustically identical to 'stepped' attn-ono but for the shuffling of the verbal  
488 prompt ordering that destroyed the consistent phase-lag associated with specific frequency  
489 bands, and supporting these Fourier-based analyses. The one potential exception is in and  
490 around posterolateral core, where there is a low-to-mid frequency progression that is similar in  
491 attn-ono and tonotopic maps, particularly in the left hemisphere. (This may be due to the small  
492 (~1 octave) overall shift in spectral mean over the course of a stimulus cycle noted in Methods).

493

494 ***Stimulus- and attentionally-driven tonotopic organization outside of auditory core.*** In line  
495 with results from previous fMRI studies (Talavage et al., 2004; Woods et al., 2009; Humphries et  
496 al., 2010; Barton et al., 2012; Dick et al., 2012; Moerel et al., 2012; Saenz and Langers, 2014;

497 Thomas et al., 2015; De Martino et al., 2015b; Ahveninen et al., 2016; Leaver and Rauschecker,  
498 2016; Riecke et al., 2016), there is stimulus-driven tonotopic mapping extending well beyond  
499 auditory core, spanning the temporal plane and continuing into the superior temporal sulcus  
500 (STS). As shown in Fig. 2a, the overall arrangement is characterized by two pairs of three  
501 interlacing best-frequency ‘fingers,’ with the high-frequency fingers (red/orange colormap)  
502 predominating medially and extending laterally, where they meet interdigitated lower-frequency  
503 fingers (green/yellow colormap) extending lateral to medial, with the longest ‘middle’ lower-  
504 frequency finger extending about halfway into auditory core. Similar to tonotopy within auditory  
505 core, the overall pattern of group activation can be observed in the majority of individual  
506 subjects (Fig. 3), but there is also considerable individual variability in the complexity,  
507 topography, and extent of tonotopic and attn-ono mapping, similar to that observed in the fMRI  
508 studies cited above (as well as electrophysiological studies in a number of studies in macaque  
509 and owl monkey, e.g., Merzenich and Brugge, 1973; Morel et al., 1993).

510

511 As can be seen in the maps in Fig. 2b, the tonotopically-aligned maps evoked by spectrally-  
512 directed attention are also present in the majority of auditory cortex outside of auditory core.  
513 Again, the structure of the tonotopic map (as revealed by Fourier analysis) is abolished when  
514 the attentional cue is randomized, thereby eliminating any consistent relationship between  
515 attended frequency band and phase lag (Fig. 2c).

516

517 The similarity between the maps evoked by presentation of a single frequency band (tonotopy)  
518 versus attention to one of two simultaneously-presented frequency bands (‘stepped’ attn-ono)  
519 can also be seen in each individual subject (Fig. 3). As with the group-averaged data, there is a  
520 close correspondence in the progression of preferred frequencies across auditory cortex in  
521 individual subjects. The similarity between the tonotopic and attn-ono maps is particularly  
522 striking in subjects 1, 2, 5, 6, and 7. The tonotopic organization of individual subjects

523 demonstrated overall commonalities, but with notable differences, even between individual  
524 subjects' right and left hemispheres, particularly outside of auditory core (Humphries et al.,  
525 2010; Moerel et al., 2014; Saenz and Langers, 2014). However, individual peculiarities were  
526 replicated across tonotopic and attn-ono conditions. In some subjects, there was a surprising  
527 lack of strong tonotopic mapping (subject 3 for which poor tonotopy may be due to greater EPI  
528 warping, and also subject 4 for which low frequencies dominated the tonotopic maps). In  
529 summary, there was a strong correspondence between tonotopic and attn-ono maps at both  
530 the group and individual levels.

531

532 **Multiple regression analyses:**

533

534 **Winner-Takes-All: Maps of 'stepped' versus 'randomized' attention conditions, and**  
535 **quantitative concordance of tonotopic and attn-ono maps.** In a complementary analysis,  
536 we used standard multiple regression techniques (see Methods) to estimate the BOLD  
537 response to each center-frequency band when it was presented in isolation (tonotopy), versus  
538 when it was attended in the presence of a distractor band (attn-ono). This allowed us to make  
539 use of the attentionally-driven signal in the randomized attn-ono condition and to combine these  
540 data with the results from the stepped attn-ono condition to increase statistical power. It also  
541 allowed us to verify that the attention effects generalize when listeners direct attention without  
542 the 'crutch' of consistent stepping up or down across attended frequency bands.

543

544 The auditory cortical patches in Fig. 4 show the cross-subject average 'Winner-Takes-All' (WTA)  
545 best frequency band (most positive-going BOLD response relative to resting baseline) maps for  
546 tonotopy and attn-ono conditions (with no shading for response amplitude). These are overlaid  
547 with the outermost  $R_1$  isocontour (dashed yellow) corresponding to auditory core. As should be  
548 expected, the topography of the WTA maps essentially recapitulates the topography revealed



549 by the phase-encoded analyses. The same holds true of the attn-tono WTA maps from both the  
550 'stepped' and importantly, the 'randomized' block conditions (Fig. 4); this result confirms that  
551 even without the 'crutch' of the stepping frequency band, listeners can direct their attention to  
552 specific frequency bands.

553

554 The WTA approach also allowed us to straightforwardly quantify the within-subject  
555 correspondence between voxel-wise best frequency, as estimated by tonotopy and by attn-tono.  
556 Here, we coded each voxel in native space as a '1' when best frequency was identical in both  
557 conditions, and a '0' otherwise. We then resampled each subject's binary maps to their cortical  
558 surface, and then averaged across subjects to create a 'concordance' map (Fig. 5a). These  
559 maps (statistically thresholded at vertex-wise  $p < 0.01$ , with surface-cluster-corrected alpha of  $p$   
560  $< 0.001$ ) show that across subjects there was high concordance across best frequency maps  
561 evoked by stimulus and by attention across much of the temporal plane in both hemispheres,  
562 with little concordance in non-auditory areas. The extent of attentionally-driven tonotopic  
563 mapping relative to overall tonotopicity is shown in the cortical patches below each concordance  
564 map in Fig. 5a. Here, the outer contour of the significant ( $p < 0.001$  clusterwise corrected)  
565 concordance map is overlaid on the phase-averaged group tonotopy map (same as Fig. 2a).  
566 Averaging over all subjects, the majority of consistently tonotopically mapped cortex medial to  
567 the crown of the superior temporal gyrus also shows preferred-frequency-aligned attn-tono  
568 maps, as does a small posterior cluster. In the left hemisphere, almost all consistently mapped  
569 tonotopic cortex also shows aligned attn-tono maps. However, it is important to note that there  
570 are considerable individual differences in regional best-frequency alignment across the tonotopy  
571 and attn-tono maps (as can be seen in Figure 3).

572

573 ***Comparison of response profiles to all frequency bands across tonotopy and attn-tono.***

574 As has been shown previously, e.g., Moerel et al., (2013), hemodynamic responses to

575 frequency in auditory cortex are not necessarily bandpass, but can be more complex and  
576 multipeaked. Therefore, we also examined whether attention to a given frequency band in the  
577 presence of a distractor band recapitulates the more graded response to non-preferred  
578 frequencies observed when that frequency band is presented in isolation. To do this, we created  
579 and surface-morphed a set of small cortical ROIs to each subject (see Fig. 5b and Methods),  
580 and quantified the similarity between the tonotopy and attn-ono response profiles in each ROI  
581 in each hemisphere by regressing the mean tonotopic parameter estimate for each frequency  
582 band against the attn-ono parameter estimate (with subjects as a random factor). We used this  
583 'ROI quilt' analysis (as opposed to a vertex-wise one) to capture regional variation in cross-  
584 condition response profile similarity across subjects, which might be obscured by individual  
585 differences in tonotopic map topography and surface-based registration errors. This also  
586 reduced the number of statistical comparisons that must be corrected for, thus increasing power  
587 to detect differences.

588

589 The region of interest (ROI) analyses (Fig. 5) further support the results from the 'concordance'  
590 maps from the Winner-Takes-All analyses (Fig. 4). The ROI analyses (Fig. 5b) show that  
591 individual subjects' tonotopy and attn-ono responses profiles are significantly associated across  
592 most of auditory cortex (all ROIs within the white border), with the exception of the most lateral  
593 aspects of the STG and upper bank of the STS. (Note that while there is a strong relationship  
594 between tonotopy and attn-ono response profiles of each subject within a given ROI, there is  
595 cross-subject variability in the particular shape of those response profiles, as suggested by the  
596 individual maps in Fig. 3). There is a broad tendency for tonotopy/attn-ono profile similarity to  
597 be strongest posterior-medially in both hemispheres, and no clear indication that profile  
598 similarity is higher in auditory core (indeed, this is not the case in the left hemisphere). As  
599 shown by the white line on the tonotopic flat maps in Fig. 5a, the area showing significant  
600 response profile similarity extends over the majority of cortex showing strong tonotopic mapping

601 with topologic similarity across subjects. The response profile similarity extends into less  
602 tonotopically consistent regions medially and posteriorly, but does not include the more postero-  
603 lateral tonotopically mapped regions along the crown of the superior temporal gyrus.

604

605 ***Loser-Takes-All: Maps of 'dis-preferred' frequency.*** Given the graded nature of frequency  
606 response preferences we observed, we suspected that there would be a large-scale topography  
607 associated with the minimum BOLD response across frequency, and that this topography would  
608 also be recapitulated by attention. Thus, we also performed a parallel 'Loser-Takes-All' (LTA)  
609 analysis, in which we coded voxels by the frequency band driving the minimum BOLD response  
610 (again relative to resting baseline) and analyzed as above. The average descriptive LTA maps  
611 show roughly opposite frequency responses compared to the WTA tonotopic maps, with higher-  
612 frequency-band-preferring regions in the tonotopic map being least driven by lower-frequency-  
613 bands, and vice versa (Fig. 6a). There is also some overlap in the 'mid-frequency-preferring'  
614 regions, likely due to blurring of values when averaging subjects' integer-based maps. There is  
615 also quite close correspondence between the frequency band evoking the least response in the  
616 tonotopy (stimulus) condition and the smallest BOLD response evoked by attending to a given  
617 frequency band. The LTA concordance maps (Fig. 6b, statistical thresholding as in Fig. 5a)  
618 show that in the right hemisphere, the alignment of tonotopic and attn-tono maps is greatest in  
619 more lateral and anterior auditory cortex, with qualitatively somewhat greater concordance more  
620 medially in the left hemisphere. (Note that the hemispheric difference and also the apparent  
621 qualitative contrast with the WTA concordance maps seen in Figures 4 and 6 are exaggerated  
622 by the cluster-wise statistical thresholding combined with the overall slightly lower concordance  
623 in the LTA maps).

624

625 ***Difference in activation across auditory areas when best frequency is attended versus***  
626 ***ignored.*** We also assessed the strength and consistency of BOLD-related frequency-band-

627 selective attention across subjects, and how the effect of attention varied with preferred or dis-  
628 preferred frequency. We first used a subject's native-space WTA map to establish each voxel's  
629 best frequency. Then, we assigned each voxel the parameter estimate for the difference in  
630 activation between attending to its best frequency in the presence of a distractor, versus  
631 attending to the distractor and ignoring its best frequency. (In other words, the value at each  
632 voxel was the estimated difference in activation between attending to, versus ignoring, its best  
633 frequency in the presence of other frequency bands). We repeated this process to estimate the  
634 parallel attention effect for each voxel's 'worst' frequency (using the corresponding LTA map).  
635 We then resampled each subject's native-space 'attention maps' to her/his cortical surface to  
636 allow for surface-based cross-subject averaging and statistical testing (all again with a vertex-  
637 wise  $p < 0.01$  threshold and surface-cluster-corrected alpha of  $p < 0.001$ ). The top row of Fig. 7  
638 shows that across subjects there was significantly greater activation across most of auditory  
639 cortex when best frequency was attended versus ignored. The widespread attention effect  
640 included all of  $R_1$ -estimated auditory core (outlined in green), extending from the inferior circular  
641 sulcus laterally to the upper bank of the STS, and antero-posteriorly from the temporal pole onto  
642 the planum temporale. By contrast, there were relatively few regions where attention to a  
643 voxel's least-preferred frequency band evoked greater activation than when the same  
644 frequency band was the distractor. Attending to a voxel's least-preferred frequency  
645 band only significantly increased activation along the posterior lateral STG in both  
646 hemispheres, extending more medially in the left, and more anteriorly in the right (Fig. 7,  
647 middle row). A direct comparison between these maps (cross-subject t-test on the difference  
648 of differences, Fig. 7, bottom row) showed that there were considerable regional differences in  
649 activation between attending to a voxel's preferred versus dis-preferred frequency band. In both  
650 hemispheres, there was greater activation across most of the anterior temporal plane when  
651 attention was directed to the preferred versus dis-preferred frequency; in the right hemisphere,

652 this effect extended throughout the temporal plane, as well as including a patch in the posterior  
653 STG. There were no regions in which the converse effect was observed (greater attend >  
654 distract activation for dis-preferred versus preferred frequency band). This shows that the  
655 frequency-selective attention-related BOLD gain is strongly modulated by frequency-preference  
656 - and provides some evidence for models of multiplicative, and not additive, attentional gain (but  
657 see Discussion).

658

659 ***Relationship of tonotopic and attn-sono map strength to MR-estimated***  
660 ***myeloarchitecture***. Typically, assays of cortical myelination are used to differentiate the most  
661 highly-myelinated cortical regions (like auditory core, MT/V5, or V1) from adjacent regions. This  
662 is true whether cortical myelination is assessed using ex-vivo 'gold-standard' approaches such  
663 as Gallyas staining, or estimated through *in-vivo* MRI T1-weighted/T2-weighted ratio,  
664 quantitative  $R_1$ , or magnetization transfer measures. However, more subtle myelination changes  
665 that occur throughout cortex may spatially correspond with changes in functional characteristics  
666 (Glasser et al., 2016; Wallace et al., 2016). For instance, recent combined fMRI and high-  
667 resolution quantitative MR show that slight reductions in cortical myelination in primary  
668 somatomotor cortex reliably occur at the border between face and hand areas (Kuehn et al.,  
669 2017).

670

671 Here, we asked whether the change in the degree to which cortex showed a strong frequency-  
672 band preference (namely, the amplitude of the phase-encoded tonotopic or attn-sono signal)  
673 spatially corresponded with changes in myelination as assessed by quantitative  $R_1$  (within a 4  
674 mm radius disk that roved across the entire cortical surface). The cross-subject-average  
675 normalized covariance map in Fig. 8a shows that there is a shared local gradient in tonotopic  
676 amplitude and  $R_1$  along the entire inferior circular sulcus and the anterior part of the superior  
677 temporal gyrus, where tonotopic amplitude and  $R_1$  drop in tandem over a narrow band of cortex.

678 There is also negative local spatial covariance between tonotopic amplitude and  $R_1$  within the  
679 center of auditory cortex, where tonotopic amplitude increases but  $R_1$  remains relatively stable.  
680 (There is also some tonotopic/ $R_1$  spatial covariance within and around the central sulcus; these  
681 regions showed considerably less overall amplitude in tonotopic response, but one that spatially  
682 covaries with changes in  $R_1$ ).

683

684 To test the replicability of this novel tonotopy-versus- $R_1$  searchlight cross-correlation, we  
685 reanalyzed  $R_1$  and tonotopy data from a previous study (Dick et al., 2012) that used a different  
686 tonotopic stimulus (bandpass-filter-swept non-linguistic vocalizations) and a slightly different  
687 multiparameter mapping protocol. Despite these methodological differences, we found a very  
688 similar pattern of tonotopic/ $R_1$  positive local spatial covariance within the circular sulcus and  
689 along the lateral STG, with negative spatial covariance again in the center of auditory cortex  
690 (Fig. 8b). The shared and relatively steep anterolateral and medial gradients in putative  
691 myelination and degree of frequency specificity - observed in two independently-acquired  
692 datasets - suggests a shared functional and myeloarchitectonic border, possibly similar in  
693 character to those reported recently relating resting state, standard task activation, and T1-  
694 weighted/T2-weighted derived myelination estimates across cortex (Glasser et al., 2016; Kuehn  
695 et al., 2017).

696

697 As seen in Fig. 8c, the spatial relationship between local  $R_1$  and *attn-tono* amplitude changes is  
698 much less clear. Here, there is a weak relationship within and around auditory cortex that is only  
699 observed within the circular sulcus (particularly in the right hemisphere). There are also stripes  
700 of spatial covariation along the banks of the central sulcus, although not closely aligned with the  
701 pattern observed with the tonotopy versus  $R_1$  covariance maps. Although very preliminary,  
702 these results suggest that changes in the degree of spectral attentional modulation in auditory  
703 cortex are not strongly linked to the underlying myeloarchitecture, and stands in contrast to the

704 consistent spatial association in lateral and medial auditory cortex between local changes in  $R_1$   
705 and the strength of stimulus-driven frequency response preference.

706

707 **Summary.** Everyday listening ordinarily takes place in rich soundscapes within multiple,  
708 simultaneous sound sources contributing to the overlapping mix of sound waves that arrives at  
709 the ears. Auditory attention is crucial to sorting out the mix. Listeners direct attentional focus to a  
710 sound source, or even to specific acoustic dimensions within a single sound source, to zero in  
711 on auditory information that is diagnostic in guiding behavior.

712

713 We asked how endogenous attention directed to specific acoustic frequency bands modulates  
714 human auditory cortical activity. Using high-resolution quantitative MRI and a novel fMRI  
715 paradigm for driving sustained selective attention within specific frequency bands, we  
716 established effects of spectrally-specific attention in myeloarchitectonically-estimated human  
717 auditory core. These effects extend across the majority of tonotopically-mapped auditory cortex,  
718 and are apparent in individual listeners. Sensory-driven best-frequency tonotopic maps align  
719 with attentionally-driven maps across much of the temporal plane, with poor concordance in  
720 non-auditory areas. Individual tonotopic and attn-ono maps show correlated idiosyncracies. The  
721 frequency bands that evoke the least BOLD response from input and from attention also exhibit  
722 close spatial correspondence. There is greater activation across most of auditory cortex when  
723 best frequency is attended, versus ignored. Finally, there is local spatial correspondence in  
724 multiple auditory regions between the degree of  $R_1$ -estimated myelination, and the strength of  
725 the frequency-band-selective fMRI response for tonotopic stimuli.

726

727

## Discussion

728



729 **Human auditory core exhibits attentionally-driven tonotopic organization.** Previous  
730 findings showed similar stimulus- and attentionally-driven frequency preference in and around  
731 Heschl's gyrus, a macroanatomical landmark associated with primary auditory areas (Da Costa  
732 et al., 2013; Riecke et al., 2016). Here, we demonstrate that, within quantitative- $R_1$ -defined  
733 primary auditory areas, the attentionally-driven maps in each hemisphere are very similar to the  
734 detailed tonotopic maps in the same subjects. As shown by comparison maps across the  
735 acoustically-identical stepped and randomized attn-ono conditions (Figs. 2 and 4), the  
736 alignment between tonotopic and attention maps depends on allocation of attention to the cued  
737 frequency band, not perceptual interference or other stimulus-driven effects. The fact that there  
738 is considerable, high-level attentional modulation within primary auditory areas is interesting  
739 given previous results suggesting more limited attentional topographic modulation in primary  
740 auditory (Atiani et al., 2014) and visual (Saygin and Sereno, 2008) cortex, compared to more  
741 robust attentional modulation in areas immediately adjacent to primary ones.

742

743 **Attentionally-driven tonotopic organization extends across much of auditory cortex.** We  
744 also find strong evidence for tonotopically-mapped spectrally-directed attention in much of  
745 auditory cortex, particularly along the lateral superior temporal gyrus (potentially analogous to  
746 lateral auditory belt and parabelt regions in macaque (Hackett, 2007)). In addition to the  
747 concordance in and around auditory core, the most consistent group-level alignment of these  
748 maps lies lateral to auditory core, with each map characterized by three higher-to-lower best-  
749 frequency-band traversals, moving from posterior to anterior roughly along the superior  
750 temporal gyrus.

751

752 This pattern suggests a cross-species parallel to results reported in ferret (Atiani et al., 2014),  
753 where task-evoked attentional modulation of frequency-tuned neurons is particularly strong in  
754 non-primary (dPEG) tonotopically mapped auditory areas in ferret. In this regard, the stimulus

755 complexity, variability, and memory demands of the current task may have helped to drive  
756 attentional response in these more lateral and anterior areas. Our results are consistent with a  
757 human fMRI comparison of cross-modal attentional effects (Petkov et al., 2004), which showed  
758 greater activation in lateral auditory regions when attention was directed to a demanding  
759 auditory repetition detection task than when the same sounds were played as subjects  
760 performed a demanding visual detection task. However, our results differ from these studies to  
761 some degree in that attentionally-driven tonotopic modulation in auditory core was also robust  
762 (similar to cross-modal attention studies in macaque A1 (O'Connell et al., 2014) and primary  
763 auditory areas (De Martino et al., 2015a)), and did not differ significantly from that in lateral belt.  
764

765 There was good correspondence between the voxel-wise best frequency-band for tonotopy and  
766 attention-tonotopy in individual listeners. Like several prior studies (data and review in  
767 Humphries et al., 2010; Moerel et al., 2014; Saenz and Langers, 2014; Brewer and Barton,  
768 2016; Leaver and Rauschecker, 2016), we observed quite substantial variation in the detailed  
769 topography of tonotopy across individuals (but cf. Ahveninen et al., 2016). It is especially  
770 noteworthy that attention-tonotopy recapitulated these topographic idiosyncrasies (as observed  
771 in the concordance analyses, Fig. 4b and 5b).

772

773 It is intriguing that there was a systematic frequency-band-associated topography not only of  
774 best frequency but also of dis-preferred frequency and, also, that the frequency-selective  
775 attenuation of BOLD gain relative to other frequencies can be recapitulated by selective  
776 attention to that frequency band in the presence of other spectral information. One could  
777 speculate that this map structure might be a population-level reflection of an 'inhibitory surround'  
778 structure observed in some electrophysiology studies (Calford and Semple, 1995; Sutter et al.,  
779 1999; but cf Wehr and Zador, 2003), with the frequency band driving the least BOLD response  
780 corresponding to the deepest trough in an asymmetric surround -- an effect that could drive the

781 very similar tonotopic and attn-sono graded frequency response preferences revealed in the  
782 multiple ROI analysis (Fig. 5b).

783

784 Here, the average frequency response profile evoked by the single-band tonotopic stimuli was  
785 recapitulated by attention to the same frequency bands in the context of distractors. Prior  
786 human neuroimaging research has been consistent with the possibility that the shape of the  
787 frequency response in and around Heschl's gyrus is attentionally-modulated in a bandpass  
788 manner that relies on amplification rather than attenuation (Riecke et al., 2016). Based on  
789 results from a larger number of spectral bands, the current findings suggest that, at least at a  
790 more macroscopic scale, spectrally-directed attention modulates cortical activity in a more  
791 graded fashion, with the shape of the attentional response to both preferred and less-preferred  
792 frequency bands similar to that evoked by stimulus alone - a contention supported by the  
793 alignment of the 'Loser-Takes-All' tonotopic and attn-sono maps (Fig. 6). That is, the frequency  
794 band that drives the smallest fMRI response when presented alone is also the frequency band  
795 that elicits the least activation when attended in the presence of a distractor. A better  
796 understanding of the mechanisms underlying these maps will require more fine-grained  
797 characterization of frequency-directed attentional modulation, preferably at very high spectral  
798 and temporal resolution (Moerel et al., 2013; Lutti et al., 2014; Moerel et al., 2014; Ahveninen et  
799 al., 2016) that might also help to unveil cortical-depth-specific attentional effects (De Martino et  
800 al., 2015a). In particular, it will be important to see whether different fMRI tasks - using more  
801 complex naturalistic sounds, or more or less abstract cues to frequency - can mimic the task-,  
802 valence- and context-dependent effects observed in non-human animal cortical auditory  
803 receptive fields, where the character of the 'contrast-enhancing' modulations differs markedly  
804 with experimental manipulation (Fritz et al., 2005; 2007a; 2007b; David et al., 2012; Atiani et al.,  
805 2014; Kuchibhotla et al., 2017). (It is worth noting that task-related modulation of frequency-  
806 selective attentional effects has long been of interest in human auditory psychophysics

807 (Greenberg, 1968; Scharf et al., 1987; Scharf, 1989; Moore et al., 1996; Green and McKeown,  
808 2001)).

809

810 ***There is correspondence between local change in  $R_1$ -estimated myelination and the***  
811 ***strength of fMRI-assessed relative frequency selectivity.*** We found that the change in the  
812 degree to which a small (4 mm radius) patch of cortex shows strong frequency preferences in  
813 tonotopy was positively spatially correlated with its degree of myelination as estimated by  $R_1$ .  
814 The strength of the correlation was anatomically specific, marking the medial border of auditory  
815 cortex (within the circular sulcus) and revealing a potential anatomical index of 'processing style'  
816 (from more to less tonotopically mapped) along anterolateral superior temporal gyrus. We found  
817 this pattern to hold true in the data from the current study as well as in an independent cohort  
818 scanned with quite different tonotopic stimuli and with multiparameter maps acquired on a  
819 different scanner model, with different sequence settings (Fig. 8c). Although there was a  
820 relatively reliable pattern of  $R_1$ -tonotopy correspondence at a group level, there was some  
821 notable individual variation in local shared  $R_1$ /tonotopy gradients relative to gyral anatomy.  
822 Thus, these patterns may be more useful than curvature for establishing areal borders on an  
823 individual subject basis, particularly when there is no obvious sharp change in a single measure  
824 (for discussion see also Glasser et al., 2016). Such work holds promise for generating novel  
825 hypotheses for more intensively characterized species like mouse, ferret, or marmoset,  
826 particularly in tandem with imaging techniques that that can cover multiple cortical areas  
827 simultaneously.

828

829 **Future Directions.** In the current study, we limited our investigation to broadly defined auditory  
830 cortex, where there was good evidence for systematic tonotopic representation from a number  
831 of previous studies (Talavage and Edmister, 2004; Hackett, 2007; Moerel et al., 2013; 2014;  
832 Saenz and Langers, 2014; Leaver and Rauschecker, 2016). In future research it will be

833 informative to examine interactions with several frontal regions whose potential analogues are  
834 known to have direct feedforward and feedback connections in macaque monkeys (Romanski  
835 and Goldman-Rakic, 2002), and where in ferret there are clear modulatory influences on  
836 primary and non-primary auditory cortex during learning (Atiani et al., 2014; Shamma and Fritz,  
837 2014). Similar to recent work in vision (Klein et al., 2014; Puckett and DeYoe, 2015), it will also  
838 be useful to establish the shape of the attentional population receptive field, and how this varies  
839 across auditory areas and relates to stimulus-driven auditory population receptive field size  
840 (Thomas et al., 2015). Finally, following on from our own pilot work, it will be exciting to explore  
841 whether higher-level auditory regionalization may follow along some of the 'fault lines' revealed  
842 by shared local tonotopic and myelin gradients, and whether or not more sophisticated and fine-  
843 grained spectral attentional manipulations may reveal a relationship between the degree of  
844 attentional malleability and underlying cortical architecture and circuitry.

845

## References

- 846  
847  
848
- 849 Ahveninen J, Chang W-T, Huang S, Keil B, Kopco N, Rossi S, Bonmassar G, Witzel T, Polimeni  
850 JR (2016) Intracortical depth analyses of frequency-sensitive regions of human auditory  
851 cortex using 7TfMRI. *NeuroImage* 143:116–127.
- 852 Atiani S, David SV, Elgueda D, Locastro M, Radtke-Schuller S, Shamma SA, Fritz JB (2014)  
853 Emergent Selectivity for Task-Relevant Stimuli in Higher-Order Auditory Cortex. *Neuron*  
854 82:486–499.
- 855 Barascud N, Pearce MT, Griffiths TD, Friston KJ, Chait M (2016) Brain responses in humans  
856 reveal ideal observer-like sensitivity to complex acoustic patterns. *Proc Natl Acad Sci*  
857 *USA* 113:E616–E625.
- 858 Barton B, Venezia JH, Saberi K, Hickok G, Brewer AA (2012) Orthogonal acoustic dimensions  
859 define auditory field maps in human cortex. *Proc Natl Acad Sci USA*.
- 860 Brewer AA, Barton B (2016) Maps of the Auditory Cortex. *Annu Rev Neurosci* 39:385–407.
- 861 Calford MB, Semple MN (1995) Monaural inhibition in cat auditory cortex. *J Neurophysiol*  
862 73:1876–1891.
- 863 Callaghan MF, Helms G, Lutti A, Mohammadi S, Weiskopf N (2014) A general linear  
864 relaxometry model of R1 using imaging data. *Magn Reson Med* 73:1309–1314.
- 865 Carey D, Caprini F, Allen M, Lutti A, Weiskopf N, Rees G, Callaghan MF, Dick F (2017)  
866 Quantitative MRI provides markers of intra-, inter-regional, and age-related differences in  
867 young adult cortical microstructure. *bioRxiv*, 139568.

- 868 Cox RW (2012) AFNI: what a long strange trip it's been. *NeuroImage* 62:743–747.
- 869 Da Costa S, van der Zwaag W, Marques JP, Frackowiak RSJ, Clarke S, Saenz M (2011)  
870 Human Primary Auditory Cortex Follows the Shape of Heschl's Gyrus. *Journal of*  
871 *Neuroscience* 31:14067–14075.
- 872 Da Costa S, Van Der Zwaag W, Miller LM, Clarke S, Saenz M (2013) Tuning in to sound:  
873 frequency-selective attentional filter in human primary auditory cortex. *Journal of*  
874 *Neuroscience* 33:1858–1863.
- 875 Dale AM, Sereno MI (1993) Improved localization of cortical activity by combining EEG and  
876 MEG with MRI cortical surface reconstruction: a linear approach. *J Cogn Neurosci*  
877 5:162–176.
- 878 David SV, Fritz JB, Shamma SA (2012) Task reward structure shapes rapid receptive field  
879 plasticity in auditory cortex. *Proc Natl Acad Sci USA* 109:2144–2149.
- 880 De Martino F, Moerel M, Ugurbil K, Goebel R, Yacoub E, Formisano E (2015a) Frequency  
881 preference and attention effects across cortical depths in the human primary auditory  
882 cortex. *Proc Natl Acad Sci USA* 112:16036–16041.
- 883 De Martino F, Moerel M, Xu J, van de Moortele PF, Ugurbil K, Goebel R, Yacoub E, Formisano  
884 E (2015b) High-Resolution Mapping of Myeloarchitecture In Vivo: Localization of  
885 Auditory Areas in the Human Brain. *Cerebral Cortex* 25:3394–3405.
- 886 Dick F, Tierney AT, Lutti A, Josephs O, Sereno MI, Weiskopf N (2012) In Vivo Functional and  
887 Myeloarchitectonic Mapping of Human Primary Auditory Areas. *Journal of Neuroscience*  
888 32:16095–16105.



- 889 Dinse J, Härtwich N, Waehnert MD, Tardif CL, Schäfer A, Geyer S, Preim B, Turner R, Bazin PL  
890 (2015) A cytoarchitecture-driven myelin model reveals area-specific signatures in human  
891 primary and secondary areas using ultra-high resolution in-vivo brain MRI. *NeuroImage*  
892 114:71–87.
- 893 Engel SA (2012) The development and use of phase-encoded functional MRI designs.  
894 *NeuroImage* 62:1195–1200.
- 895 Engel SA, Rumelhart DE, Wandell BA, Lee AT, Glover GH, Chichilnisky EJ, Shadlen MN (1994)  
896 fMRI of human visual cortex. *Nature* 369:525.
- 897 Feinberg DA, Moeller S, Smith SM, Auerbach E, Ramanna S, Glasser MF, Miller KL, Ugurbil K,  
898 Yacoub E (2010) Multiplexed Echo Planar Imaging for Sub-Second Whole Brain fMRI  
899 and Fast Diffusion Imaging Valdes-Sosa PA, ed. *PLoS ONE* 5:e15710.
- 900 Feinberg DA, Setsompop K (2013) Ultra-fast MRI of the human brain with simultaneous multi-  
901 slice imaging. *Journal of Magnetic Resonance* 229:90–100.
- 902 Fischl B, Sereno MI, Tootell RB, Dale AM (1999) High-resolution intersubject averaging and a  
903 coordinate system for the cortical surface. *Hum Brain Mapp* 8:272–284.
- 904 Fritz JB, David SV, Radtke-Schuller S, Yin P, Shamma SA (2010) Adaptive, behaviorally gated,  
905 persistent encoding of task-relevant auditory information in ferret frontal cortex. *Nature*  
906 *Neuroscience* 13:1011–1019.
- 907 Fritz JB, Elhilali M, David SV, Shamma SA (2007a) Does attention play a role in dynamic  
908 receptive field adaptation to changing acoustic salience in A1? *Hear Res* 229:186–203.
- 909 Fritz JB, Elhilali M, Shamma SA (2005) Differential dynamic plasticity of A1 receptive fields  
910 during multiple spectral tasks. *J Neurosci* 25:7623–7635.

- 911 Fritz JB, Elhilali M, Shamma SA (2007b) Adaptive changes in cortical receptive fields induced  
912 by attention to complex sounds. *J Neurophysiol* 98:2337–2346.
- 913 Glasser MF, Coalson TS, Robinson EC, Hacker CD, Harwell J, Yacoub E, Ugurbil K, Andersson  
914 J, Beckmann CF, Jenkinson M, Smith SM, Van Essen DC (2016) A multi-modal  
915 parcellation of human cerebral cortex. *Nature*:1–11.
- 916 Green TJ, McKeown JD (2001) Capture of attention in selective frequency listening. *J Exp*  
917 *Psychol Hum Percept Perform* 27:1197–1210.
- 918 Greenberg GZ (1968) Frequency-Response Characteristic of Auditory Observers Detecting  
919 Signals of a Single Frequency in Noise: The Probe-Signal Method. *J Acoust Soc Am*  
920 44:1513.
- 921 Greve DN, Fischl B (2009) Accurate and robust brain image alignment using boundary-based  
922 registration. *NeuroImage* 48:63–72.
- 923 Hackett TA, Preuss TM, Kaas JH (2001) Architectonic identification of the core region in  
924 auditory cortex of macaques, chimpanzees, and humans. *J Comp Neurol* 441:197–222.
- 925 Hackett TA (2007) Organization and Correspondence of the Auditory Cortex of Humans and  
926 Nonhuman Primates. *Evolution of the Nervous System*, JH Kaas, Ed:109–119. Hagler D,  
927 Saygin A, Sereno M (2006) Smoothing and cluster thresholding for cortical surface-  
928 based group analysis of fMRI data. *NeuroImage* 33:1093–1103.
- 929 Hagler DJ Jr, Sereno MI (2006) Spatial maps in frontal and prefrontal cortex. *NeuroImage*  
930 29:567–577.
- 931 Hagler DJ, Riecke L, Sereno MI (2007) Parietal and superior frontal visuospatial maps activated  
932 by pointing and saccades. *NeuroImage* 35:1562–1577.

- 933 Helms G, Dathe H, Dechent P (2008) Quantitative FLASH MRI at 3T using a rational  
934 approximation of the Ernst equation. *Magn Reson Med* 59:667–672.
- 935 Helms G, Draganski B, Frackowiak R, Ashburner J, Weiskopf N (2009) Improved segmentation  
936 of deep brain grey matter structures using magnetization transfer (MT) parameter maps.  
937 *NeuroImage* 47:194–198.
- 938 Herdener M, Esposito F, Scheffler K, Schneider P, Logothetis NK, Uludağ K, Kayser C (2013)  
939 Spatial representations of temporal and spectral sound cues in human auditory cortex.  
940 *Cortex* 49:2822–2833.
- 941 Herrmann B, Henry MJ (2013) Frequency-specific adaptation in human auditory cortex depends  
942 on the spectral variance in the acoustic stimulation. *Journal of ....*
- 943 Humphries C, Liebenthal E, Binder JR (2010) Tonotopic organization of human auditory cortex.  
944 *NeuroImage* 50:1202–1211.
- 945 Idemaru K, Holt LL (2011) Word recognition reflects dimension-based statistical learning. *J Exp*  
946 *Psychol Hum Percept Perform* 37:1939–1956.
- 947 Kastner S, Ungerleider LG (2000) Mechanisms of visual attention in the human cortex. *Annu*  
948 *Rev Neurosci* 23:315–341.
- 949 Klein BP, Harvey BM, Dumoulin SO (2014) Attraction of Position Preference by Spatial Attention  
950 throughout Human Visual Cortex. *Neuron* 84:227–237.
- 951 Kuchibhotla KV, Gill JV, Lindsay GW, Papadoyannis ES, Field RE, Sten TAH, Miller KD,  
952 Froemke RC (2017) Parallel processing by cortical inhibition enables context-dependent  
953 behavior. *Nature Neuroscience* 20:62–71.

- 954 Kuehn E, Dinse J, Jakobsen E, Long X, Schäfer A, Bazin P-L, Villringer A, Sereno MI, Margulies  
955 DS (2017) Body Topography Parcellates Human Sensory and Motor Cortex. *Cerebral*  
956 *Cortex*:1–16.
- 957 Langers DRM, Krumbholz K, Bowtell RW, Hall DA (2014) Neuroimaging paradigms for tonotopic  
958 mapping (I): the influence of sound stimulus type. *NeuroImage* 100:650–662.
- 959 Langers DRM, van Dijk P (2012) Mapping the tonotopic organization in human auditory cortex  
960 with minimally salient acoustic stimulation. *Cerebral Cortex* 22:2024–2038.
- 961 Leaver AM, Rauschecker JP (2016) Functional Topography of Human Auditory Cortex. *Journal*  
962 *of Neuroscience* 36:1416–1428.
- 963 Lutti A, Dick F, Sereno MI, Weiskopf N (2014) Using high-resolution quantitative mapping of R1  
964 as an index of cortical myelination. *NeuroImage* 93 Pt 2:176–188.
- 965 Lutti A, Hutton C, Finsterbusch J, Helms G, Weiskopf N (2010) Optimization and validation of  
966 methods for mapping of the radiofrequency transmit field at 3T. *Magn Reson Med*  
967 64:229–238.
- 968 Lutti A, Stadler J, Josephs O, Windischberger C, Speck O, Bernarding J, Hutton C, Weiskopf N  
969 (2012) Robust and fast whole brain mapping of the RF transmit field B1 at 7T. *PLoS*  
970 *ONE* 7:e32379.
- 971 Merzenich MM, Brugge JF (1973) Representation of the cochlear partition of the superior  
972 temporal plane of the macaque monkey. *Brain Res* 50:275–296.
- 973 Moerel M, De Martino F, Formisano E (2012) Processing of Natural Sounds in Human Auditory  
974 Cortex: Tonotopy, Spectral Tuning, and Relation to Voice Sensitivity. *Journal of*  
975 *Neuroscience* 32:14205–14216.

- 976 Moerel M, De Martino F, Formisano E (2014) An anatomical and functional topography of  
977 human auditory cortical areas. *Frontiers in Neuroscience* 8.
- 978 Moerel M, De Martino F, Santoro R, Ugurbil K, Goebel R, Yacoub E, Formisano E (2013)  
979 Processing of natural sounds: characterization of multipeak spectral tuning in human  
980 auditory cortex. *Journal of Neuroscience* 33:11888–11898.
- 981 Moore BCJ, Hafter ER, Glasberg BR (1996) The probe-signal method and auditory-filter shape:  
982 Results from normal- and hearing-impaired subjects. *J Acoust Soc Am* 99:542–552.
- 983 Morel A, Garraghty PE, Kaas JH (1993) Tonotopic organization, architectonic fields, and  
984 connections of auditory cortex in macaque monkeys. *J Comp Neurol* 335:437–459.
- 985 Morosan P, Rademacher J, Schleicher A, Amunts K, Schormann T, Zilles K (2001) Human  
986 primary auditory cortex: cytoarchitectonic subdivisions and mapping into a spatial  
987 reference system. *NeuroImage* 13:684–701.
- 988 O'Connell MN, Barczak A, Schroeder CE, Lakatos P (2014) Layer Specific Sharpening of  
989 Frequency Tuning by Selective Attention in Primary Auditory Cortex. *Journal of*  
990 *Neuroscience* 34:16496–16508.
- 991 Oh J, Kwon JH, Yang PS, Jeong J (2013) Auditory imagery modulates frequency-specific areas  
992 in the human auditory cortex. *J Cogn Neurosci* 25:175–187.
- 993 Paltoglou AE, Sumner CJ, Hall DA (2009) Examining the role of frequency specificity in the  
994 enhancement and suppression of human cortical activity by auditory selective attention.  
995 *Hear Res* 257:106–118.
- 996 Petkov CI, Kang X, Alho K, Bertrand O, Yund EW, Woods DL (2004) Attentional modulation of  
997 human auditory cortex. *Nature Neuroscience* 7:658–663.

- 998 Pierpaoli C (2010) Quantitative Brain MRI. *Topics in Magnetic Resonance Imaging*, 21:63.
- 999 Preibisch C, Deichmann R (2009) Influence of RF spoiling on the stability and accuracy of T1  
1000 mapping based on spoiled FLASH with varying flip angles. *Magn Reson Med* 61:125–  
1001 135.
- 1002 Puckett AM, DeYoe EA (2015) The Attentional Field Revealed by Single-Voxel Modeling of fMRI  
1003 Time Courses. *Journal of Neuroscience* 35:5030–5042.
- 1004 Rao AA, Talavage TM (2005) Reliability of phase-encode mapping in the presence of spatial  
1005 non-stationarity of response latency. *NeuroImage* 28:563–578.
- 1006 Riecke L, Peters JC, Valente G, Kemper VG, Formisano E, Sorger B (2016) Frequency-  
1007 Selective Attention in Auditory Scenes Recruits Frequency Representations Throughout  
1008 Human Superior Temporal Cortex. *Cerebral Cortex*.
- 1009 Romanski LM, Goldman-Rakic PS (2002) An auditory domain in primate prefrontal cortex.  
1010 *Nature Neuroscience* 5:15–16.
- 1011 Saenz M, Langers DRM (2014) Tonotopic mapping of human auditory cortex. *Hear Res*  
1012 307:42–52.
- 1013 Saygin AP, Sereno MI (2008) Retinotopy and attention in human occipital, temporal, parietal,  
1014 and frontal cortex. *Cereb Cortex* 18:2158–2168.
- 1015 Scharf B (1989) Spectral specificity in auditory detection: The effect of listening on hearing.  
1016 *Journal of the Acoustical Society of Japan* (E).
- 1017 Scharf B, Quigley S, Aoki C, Peachey N, Reeves A (1987) Focused auditory attention and  
1018 frequency selectivity. *Percept Psychophys* 42:215–223.

- 1019 Schönwiesner M, Zatorre RJ (2009) Spectro-temporal modulation transfer function of single  
1020 voxels in the human auditory cortex measured with high-resolution fMRI. *Proc Natl Acad*  
1021 *Sci USA* 106:14611–14616.
- 1022 Schwarzkopf DS, Song C, Rees G (2011) The surface area of human V1 predicts the subjective  
1023 experience of object size. *Nature Neuroscience* 14:28–30.
- 1024 Sereno MI, Dale AM, Reppas JB, Kwong KK, Belliveau JW, Brady TJ, Rosen BR, Tootell RB  
1025 (1995) Borders of multiple visual areas in humans revealed by functional magnetic  
1026 resonance imaging. *Science (New York, NY)* 268:889–893.
- 1027 Sereno MI, Huang R-S (2006) A human parietal face area contains aligned head-centered  
1028 visual and tactile maps. *Nature Neuroscience* 9:1337–1343.
- 1029 Sereno MI, Lutti A, Weiskopf N, Dick F (2013) Mapping the human cortical surface by combining  
1030 quantitative T(1) with retinotopy. *Cerebral Cortex* 23:2261–2268.
- 1031 Shamma S, Fritz J (2014) Adaptive auditory computations. *Curr Opin Neurobiol* 25:164–168.
- 1032 Smith SM, Jenkinson M, Woolrich MW, Beckmann CF, Behrens TEJ, Johansen-Berg H,  
1033 Bannister PR, De Luca M, Drobnjak I, Flitney DE, Niazy RK, Saunders J, Vickers J,  
1034 Zhang Y, De Stefano N, Brady JM, Matthews PM (2004) Advances in functional and  
1035 structural MR image analysis and implementation as FSL. *NeuroImage* 23:S208–S219.
- 1036 Stüber C, Morawski M, Schäfer A, Labadie C, Wähnert M, Leuze C, Streicher M, Barapatre N,  
1037 Reimann K, Geyer S, Spemann D, Turner R (2014) Myelin and iron concentration in the  
1038 human brain: A quantitative study of MRI contrast. *NeuroImage*.

- 1039 Sutter ML, Schreiner CE, McLean M, O'Connor KN, Loftus WC (1999) Organization of Inhibitory  
1040 Frequency Receptive Fields in Cat Primary Auditory Cortex. *J Neurophysiol* 82:2358–  
1041 2371.
- 1042 Sweet RA, Dorph-Petersen K-A, Lewis DA (2005) Mapping auditory core, lateral belt, and  
1043 parabelt cortices in the human superior temporal gyrus. *J Comp Neurol* 491:270–289.
- 1044 Talavage TM, Edmister WB (2004) Nonlinearity of fMRI responses in human auditory cortex.  
1045 *Hum Brain Mapp* 22:216–228.
- 1046 Talavage TM, Sereno MI, Melcher JR, Ledden PJ, Rosen BR, Dale AM (2004) Tonotopic  
1047 organization in human auditory cortex revealed by progressions of frequency sensitivity.  
1048 *J Neurophysiol* 91:1282–1296.
- 1049 Tardif CL, Gauthier CJ, Steele CJ, Bazin P-L, Schäfer A, Schaefer A, Turner R, Villringer A  
1050 (2016) Advanced MRI techniques to improve our understanding of experience-induced  
1051 neuroplasticity. *NeuroImage* 131:55–72.
- 1052 Tardif CL, Schäfer A, Waehnert M, Dinse J, Turner R, Bazin P-L (2015) Multi-contrast multi-  
1053 scale surface registration for improved alignment of cortical areas. *NeuroImage*  
1054 111:107–122.
- 1055 Thomas JM, Huber E, Stecker GC, Boynton GM, Saenz M, Fine I (2015) Population receptive  
1056 field estimates of human auditory cortex. *NeuroImage* 105:428–439.
- 1057 Turner R (2015) Myelin imaging. In: *Brain mapping: An encyclopedic reference*, pp 137–142.  
1058 Academic Press: Elsevier.



- 1059 Wallace M, Cronin M, Bowtell RW, Scott I, Palmer AR, Gowland P (2016) Histological Basis of  
1060 Laminar MRI Patterns in High Resolution Images of Fixed Human Auditory Cortex.  
1061 Frontiers in Neuroscience.
- 1062 Wehr M, Zador AM (2003) Balanced inhibition underlies tuning and sharpens spike timing in  
1063 auditory cortex. Nature 426:442–446.
- 1064 Woods DL, Stecker GC, Rinne T, Herron TJ, Cate AD, Yund EW, Liao I, Kang X (2009)  
1065 Functional maps of human auditory cortex: effects of acoustic features and attention.  
1066 PLoS ONE 4:e5183.
- 1067

## Figure Captions

1068

1069

1070 **Figure 1. Stimuli and design overview.** (A) In a representative 12.8s **Tonotopy block** a  
1071 neutral verbal prompt “*hear*” precedes 14 four-tone mini-sequences sampled around one of 5  
1072 center frequencies. The task is to detect the 1-3 mini-sequence repeats embedded within the  
1073 block. The grey box highlights a single mini-sequence repeat. (B) A single **Attention-Tonotopy**  
1074 **(Attn-tono) block** includes two simultaneous streams of mini-sequences with distinct center  
1075 frequencies. Mini-sequence repeats occur in each stream. A verbal prompt (“*high*” or “*low*”)  
1076 directs listeners to attend to one stream and report mini-sequence repeats in that stream, while  
1077 ignoring repeats in the unattended stream. Two randomly-ordered orientation tones at the  
1078 center frequency of each stream alert listeners to the frequency neighborhood of the upcoming  
1079 streams. (C) A single 64s **cycle of Stepped Attn-tono blocks** includes five 12.8s blocks that  
1080 step up (shown), or down, in center frequency. In this single cycle, the frequency band to which  
1081 attention is directed by the verbal prompt (indicated with “*high*”/“*low*” above each block) is  
1082 acoustically matched with the Tonotopy cycle shown in (B), but there are always competing  
1083 unattended mini-sequences in a distinct frequency band. (D) A single 64s **cycle of**  
1084 **Randomized Attn-tono blocks** is acoustically identical to the Stepped Attn-tono cycle in (C),  
1085 except that half of the verbal prompts have been swapped, and therefore no longer cue  
1086 attention to frequency with consistent phase lags. (E) The distinction between Stepped and  
1087 Randomized Attn-tono blocks is highlighted by examining the first three (of eight) **cycles of a**  
1088 **Stepped (top) versus Randomized (bottom) Attn-tono run.** The focus of attention is color  
1089 coded in the frequency-band-specific manner shown in (A). For the Stepped condition (top),  
1090 there is a consistent relationship between the stimulus phase lag and the attended frequency  
1091 across cycles within a run. Thus, for voxels that show a consistently higher response at one  
1092 attended frequency band compared to all others, there will be a periodic response at 8  
1093 cycles/run at a given phase lag corresponding to the particular frequency band attended. For

1094 the Randomized condition (bottom), there is no consistent relationship, providing a control  
1095 condition for Fourier analyses because frequency-band-directed attention is aperiodic across a  
1096 run. **(F)** The stimulus phase lag with the highest periodic BOLD signal amplitude is determined  
1097 for each voxel, mapped to a color scale, and then painted onto the cortical surface patch. BOLD  
1098 signal amplitude is mapped to the color's saturation. (Note: In these panels A-D, stimulus  
1099 intensity is adjusted across the spectrum to aid visual presentation of energy across frequency  
1100 bands. See Methods for details on actual intensity across frequency bands).

1101

1102 **Figure 2. Group activation for Tonotopy and Attention-Tonotopy conditions, with  $R_1$**   
1103 **contours showing putative auditory core.** The left-most panel shows cortical-surface-based  
1104 group-averaged  $R_1$ , projected on the lateral inflated surface of one subject. (The left hemisphere  
1105 is mirror-reversed to align cortical maps for visual comparison). For tonotopic map display, a  
1106 patch of cortex including the entire temporal plane (shown in purple on the inflated surface) was  
1107 cut and flattened. Panels A-C show this region enlarged, with isocontour lines showing  
1108 quantitative  $R_1$  values for the group-averaged putative auditory core, and color maps showing  
1109 group-averaged best frequency as a function of **(A)** Tonotopy, **(B)** Attn-ono (Stepped), and **(C)**  
1110 Attn-ono (Randomized Control) conditions. The stars are fiduciary points to assist in visual  
1111 comparisons of maps across conditions; the outline of Heschl's gyrus is in yellow dashed lines  
1112 (in **(A)**, from the individual subject whose cortical patch was used). Consistent with previous  
1113 work, the tonotopic map is characterized by two pairs of three interlacing best-frequency  
1114 'fingers,' with the high-frequency fingers (red/orange colormap) showing greatest frequency  
1115 preference medially and extending laterally, where they meet interdigitated lower-frequency  
1116 fingers (green/yellow colormap) extending lateral to medial, with the longest 'middle' lower-  
1117 frequency finger extending about halfway into auditory core. This pattern is evident in Fourier-  
1118 analysis-derived maps of the 'stepped' Attn-ono condition but not in the 'randomized control'  
1119 Attn-ono condition, for which the attentional response was phase-cancelled. All maps are

1120 statistically masked by overall activation to tonotopy stimuli in each hemisphere (cluster-  
1121 corrected  $p < 10^{-8}$ , and gently shaded to show relative amplitude).

1122

1123 **Figure 3. Individual subjects' Tonotopy and Attention-Tonotopy maps.** Each subject's  
1124 Tonotopic and Attn-Tono (Stepped) Fourier-analysis-derived maps are displayed on the same  
1125 subject's flattened superior temporal cortical patch.  $R_1$  isocontours around presumptive auditory  
1126 core are shown in white, with thick solid lines depicting the lowest-valued (outermost)  $R_1$   
1127 isocontour, thin solid lines depicting the highest (innermost)  $R_1$  isocontour, and dashed lines  
1128 showing intermediate values. ( $R_1$  values differ somewhat across individuals). Dashed black lines  
1129 indicate the outline of the cortical-surface-morphed 'TE1.0' label, where the area inside the line  
1130 contains vertices estimated to have a  $p > 0.3$  probability of falling within primary auditory cortex  
1131 based on the Morosan et al., (2001) postmortem probability atlas (see Methods). Activation  
1132 maps are gently shaded to show changes in response amplitude, but are unthresholded for  
1133 comparison with individual maps from previous studies, e.g., Da Costa et al., (2011).

1134

1135 **Figure 4. Comparison of responses in regression-based 'Winner-Takes-All' maps,**  
1136 **Tonotopy and Attn-Tono.** The color maps projected onto the right (*top panels*) and left (*bottom*  
1137 *panels*) hemisphere cortical patches (same as patches shown in purple in Figure 2) show the  
1138 cross-subject average best frequency band ('Winner-Takes-All,' or WTA) for 'stepped' tonotopic  
1139 (left) 'stepped' attn-tono (middle) and 'randomized' attn-tono conditions. Note that with the  
1140 regression-based approach, the 'randomized' condition is also expected to evoke strong  
1141 attentionally-driven tonotopic maps. The dotted yellow line depicts the outermost  $R_1$  contour  
1142 ( $0.66 \text{ sec}^{-1}$ ) around presumptive auditory core as shown in Figure 2.

1143

1144 **Figure 5. Comparison of Tonotopy and Attn-tono maps. (A)** 'Concordance maps' are  
1145 rendered in heatscale on the inflated hemispheres to illustrate the similarity in best frequency

1146 between tonotopic and attn-ono maps (the latter averaged over stepped and randomized  
1147 blocks). These maps were calculated in two stages. First, in each subject's native EPI space, a  
1148 voxel was coded as '1' if tonotopy and attn-ono stimuli evoked the same best frequency, and  
1149 otherwise coded as '0'. Second, for each subject, the concordance maps were resampled to the  
1150 individual's cortical surface, and projected onto the unit icosahedron for cross-subject surface-  
1151 based averaging, thereby creating a composite measure of agreement between tonotopy and  
1152 attn-ono maps, weighted by the consistency of this agreement across subjects. The  
1153 concordance maps are statistically masked with a cross-subject t-map, calculated versus  
1154 chance agreement ( $p=0.20$ ) with a surface cluster correction of  $p < 0.001$  (vertex-wise  $p < 0.01$ ,  
1155 cluster threshold surface area  $> 74 \text{ mm}^2$ , (Hagler et al., 2006). To demonstrate the extent of  
1156 tonotopically-mapped cortex that is similarly mapped through spectrally-directed attention, the  
1157 phase-encoded tonotopy cortical patches from Figure 2a are overlaid with the outline of the  
1158 thresholded concordance map shown by the yellow dotted line. The white solid outline shows  
1159 the Bonferroni-corrected ROI-wise correspondence outline from the 'ROI quilt' in panel B **(B)**  
1160 The shading in each small ROI patch shows the z-score for the partial fit between tonotopy and  
1161 attn-ono responses to each frequency band (with subjects as a random factor). ROIs with  
1162 significant z-scores (Bonferroni-corrected p-value threshold of  $p < 0.05$ ) are indicated by the thin  
1163 white outline.

1164

1165 **Figure 6. Comparison of responses in regression-based 'Loser-Takes-All' maps,**  
1166 **Tonotopy and Attn-ono.** (A) The colormaps projected onto the same cortical patches as  
1167 Figures 2 and 4 show cross-subject group-average maps that depict the frequency band that  
1168 drives the *least activation* compared to all other frequency bands ('Loser-Takes-All', or LTA) in  
1169 tonotopy and attn-ono (stepped plus randomized blocks) conditions and in right and left  
1170 hemispheres. As in Figure 4, the presumptive auditory core shown by the dashed yellow line  
1171 depicting the outermost  $R_1$  contour ( $0.66 \text{ sec}^{-1}$ ). (B) The tonotopy versus attn-ono LTA

1172 concordance map was created as in Figure 5a; note that the midpoint of the heatscale has been  
1173 lowered slightly compared to Figure 5a, reflecting the overall somewhat lower concordance in  
1174 the LTA maps compared to WTA. The dotted yellow  $R_1$  isocontour is the same as Figure 4.

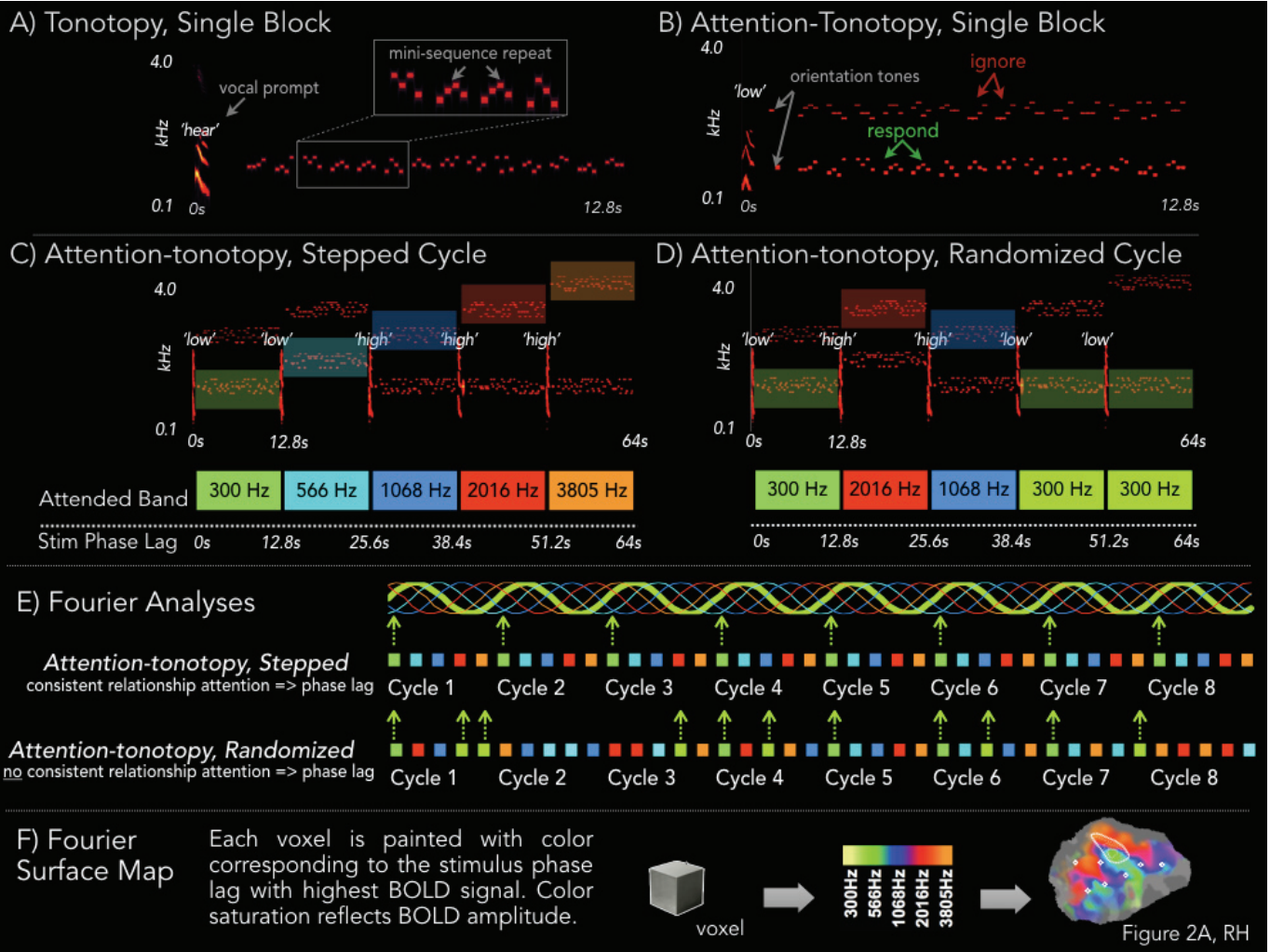
1175

1176 **Figure 7. Comparison of maps when best frequency is attended versus ignored.** The  
1177 heatscale (t-values, thresholded as in Figure 5a) depicts the cross-subject cortical-surface-  
1178 based average difference in activation when the subject-specific best frequency band of each  
1179 voxel was attended versus ignored. The dotted green  $R_1$  isocontour estimating auditory core is  
1180 as in Figure 4.

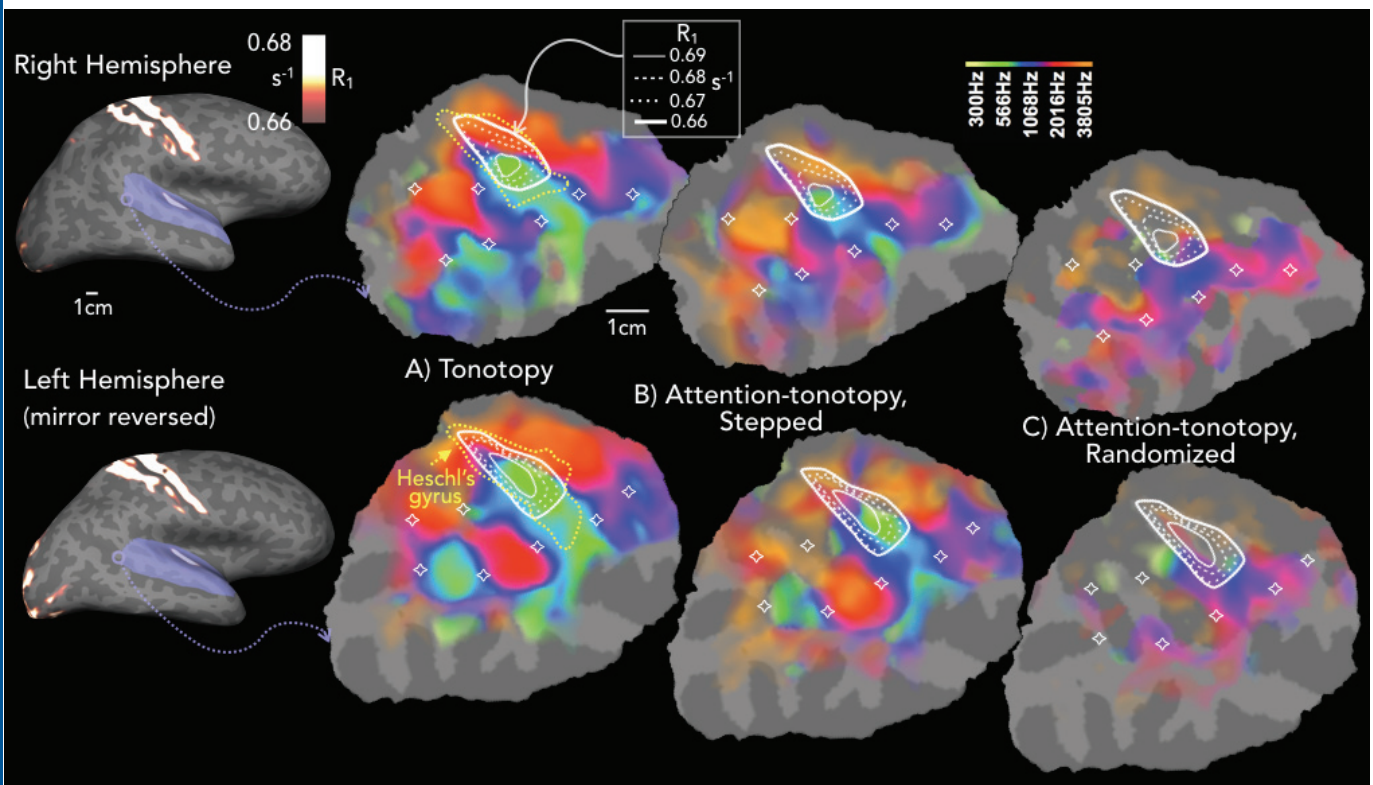
1181

1182 **Figure 8. Local normalized covariance between  $R_1$  values and tonotopic and attn- tono**  
1183 **response amplitude.** The heatscale value at each vertex represents the normalized spatial  
1184 covariance within a 4mm (2D) radius between  $R_1$  and the amplitude of the tonotopic or attn-  
1185 tono signal (e.g., the amplitude of the Fourier component at the stimulus frequency of 8  
1186 cycles/run). **(A)** The cross-subject (N=8) cortical-surface-based average normalized covariance  
1187 between  $R_1$  and tonotopic amplitude. **(B)** The  $R_1$  versus tonotopy normalized covariance in an  
1188 independent cohort (N=6), using data previously acquired with a different tonotopy protocol  
1189 (bandpass-filter-swept non-linguistic vocalizations) and on a different scanner (Siemens 3T  
1190 Trio); full protocol as described in Dick et al., (2012). **(C)** The average normalized covariance  
1191 between  $R_1$  and attn-tono amplitude in the current cohort.

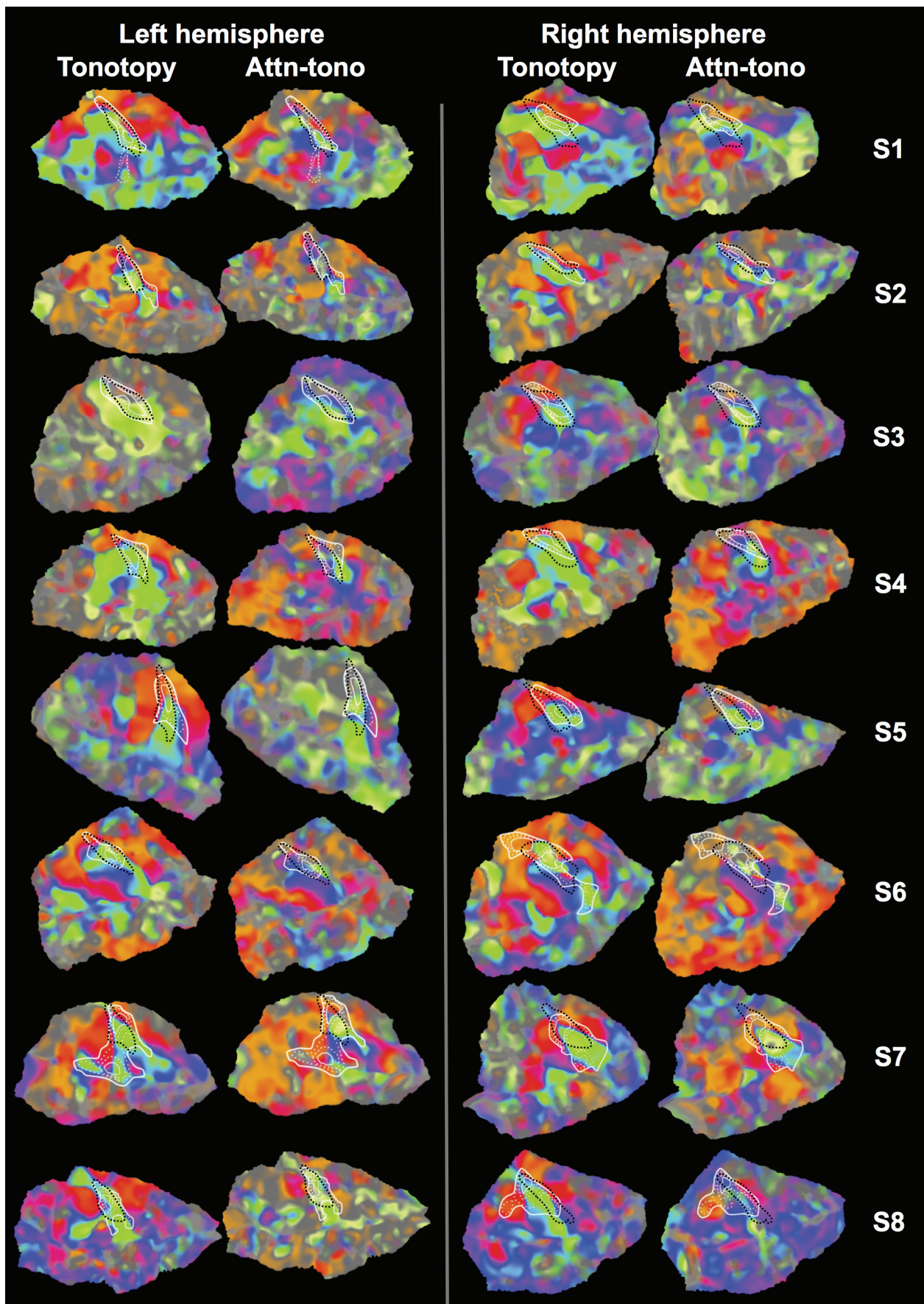
1192

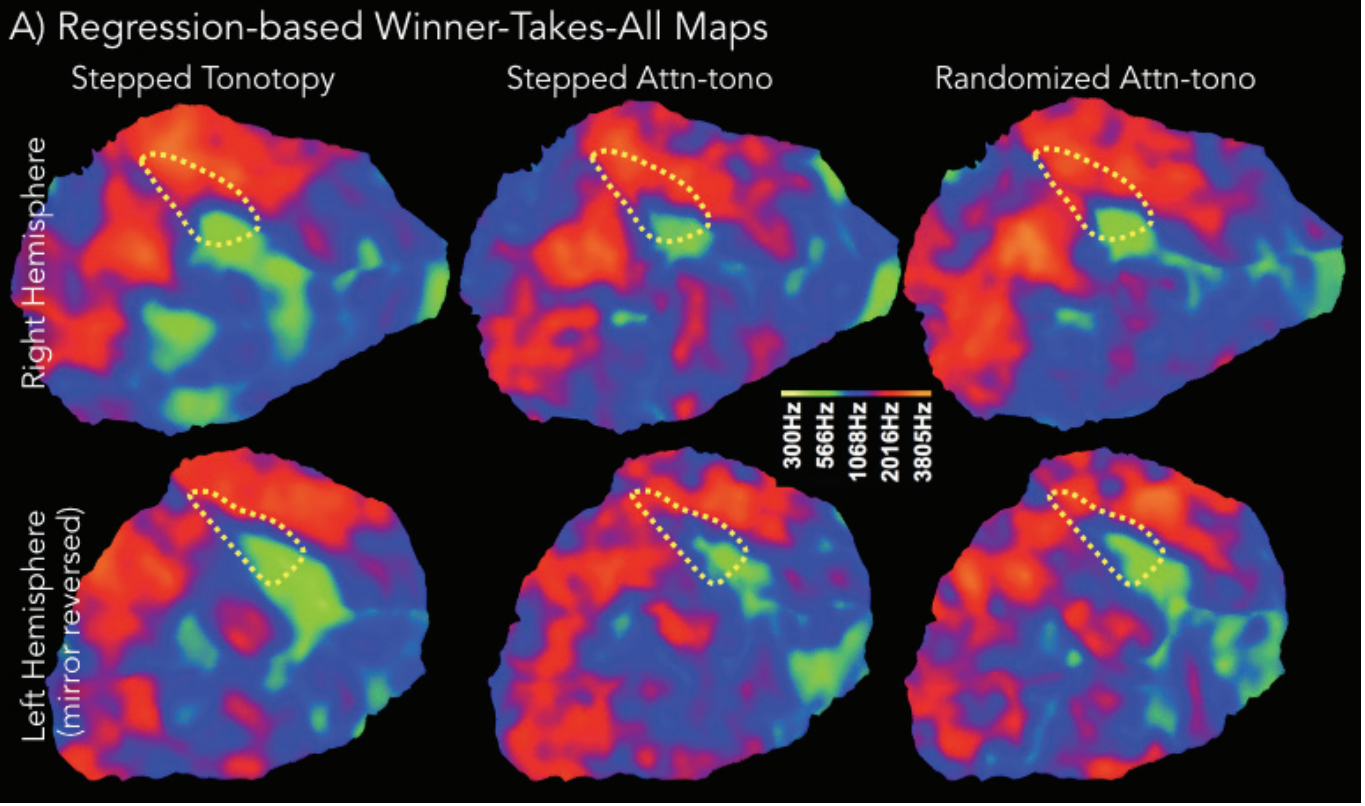






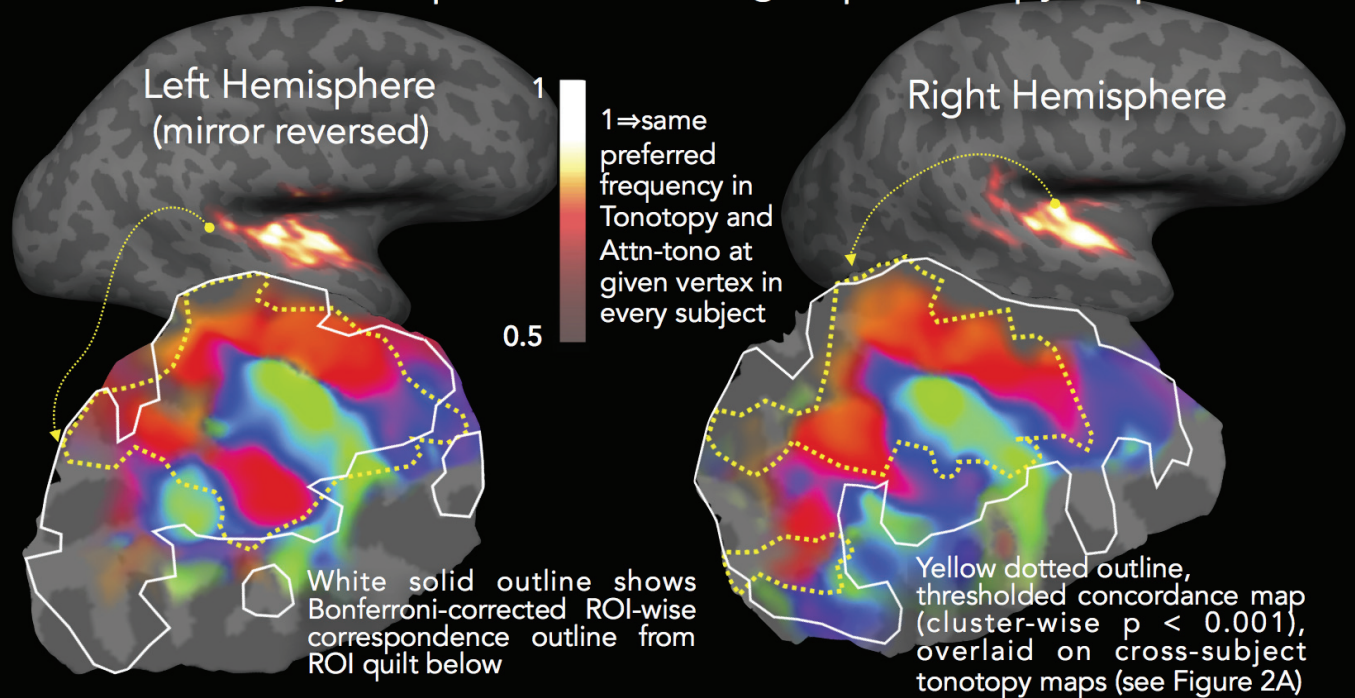




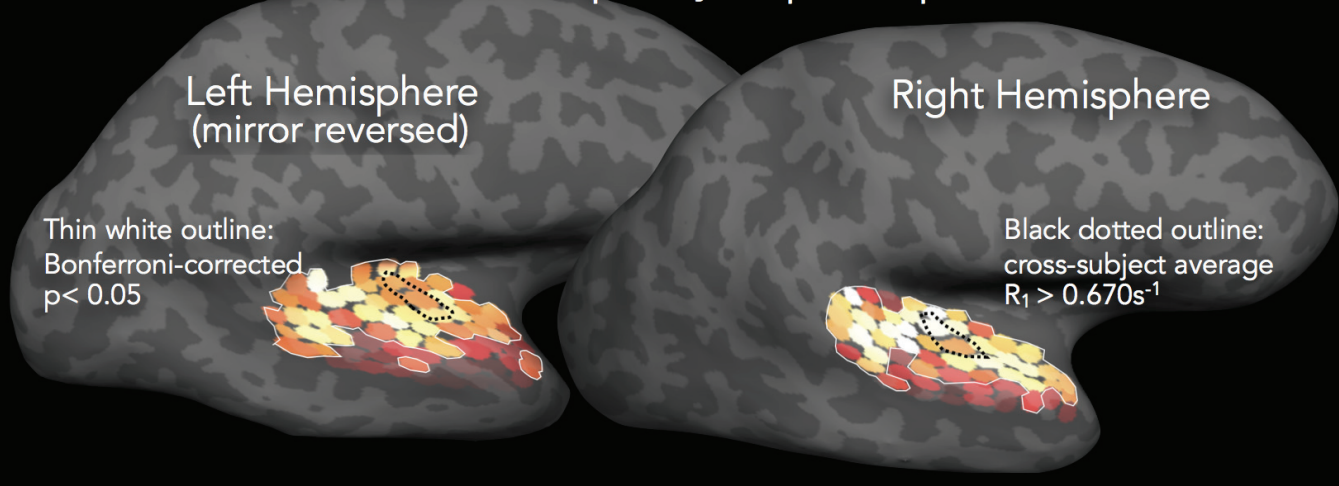




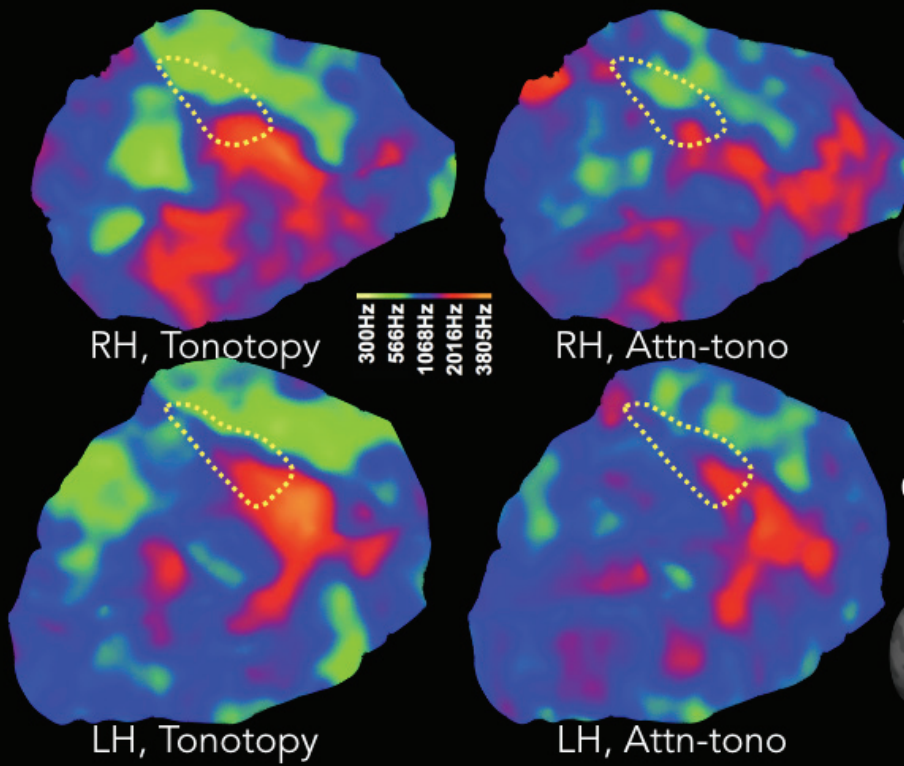
### A) Concordance Maps, Tonotopy vs Attn-tono: Overlay on phase-encoded group tonotopy maps



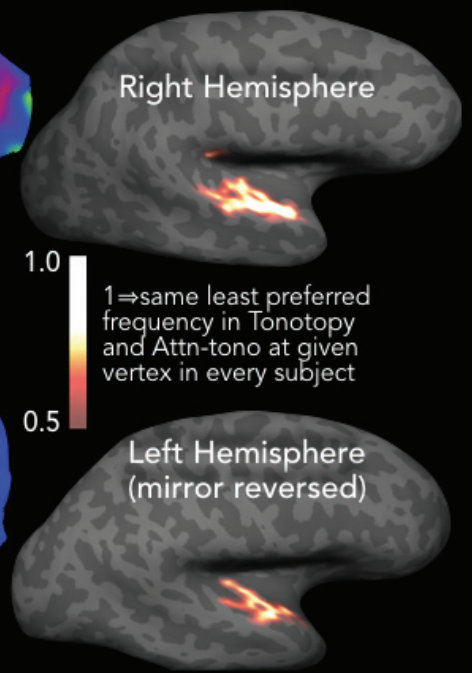
### B) ROI-wise correspondence between Tonotopy and Attn-tono frequency response profiles

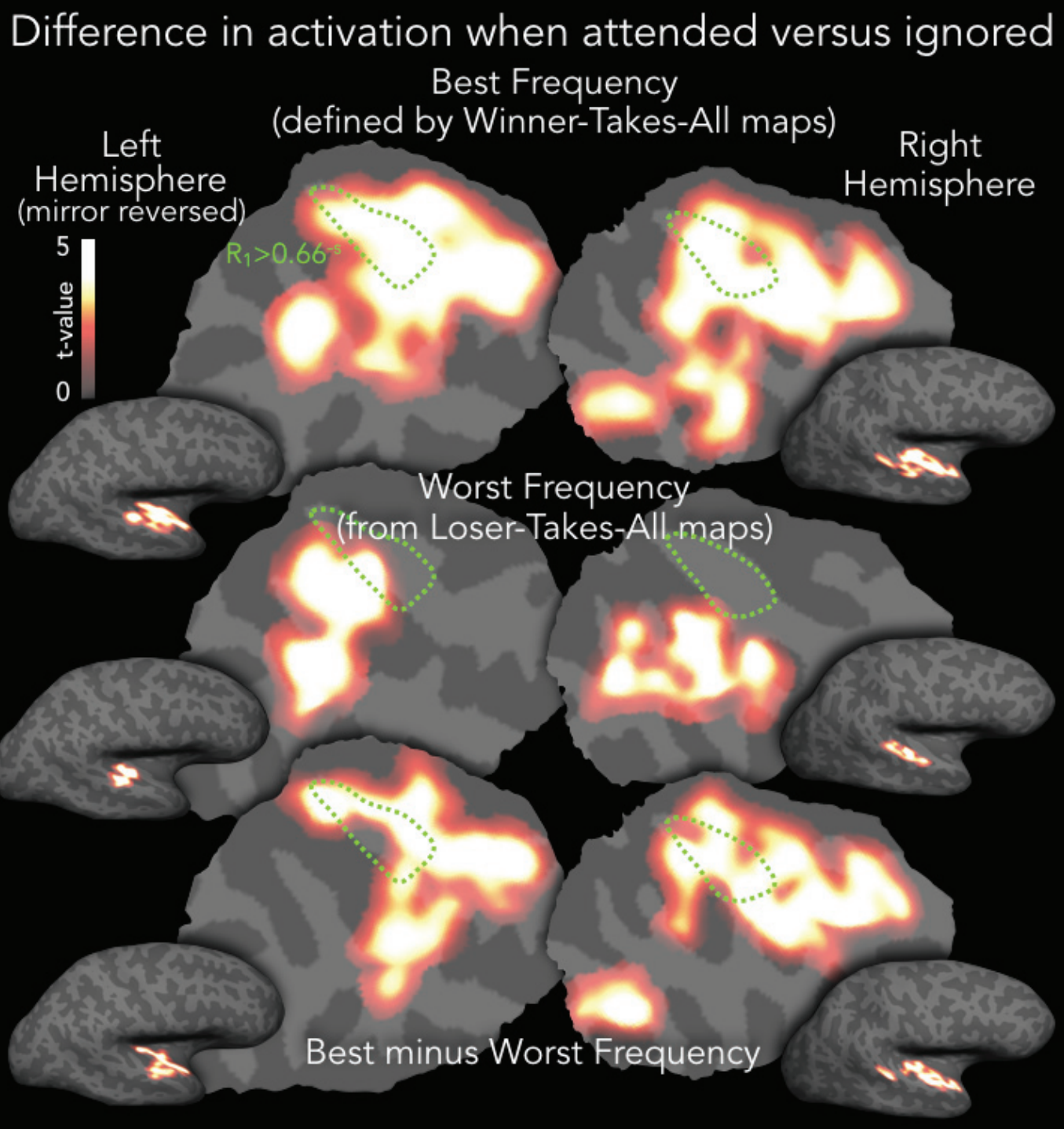


A) Regression-based Loser-Takes-All Maps



B) Concordance maps, Tonotopy vs Attn-tono

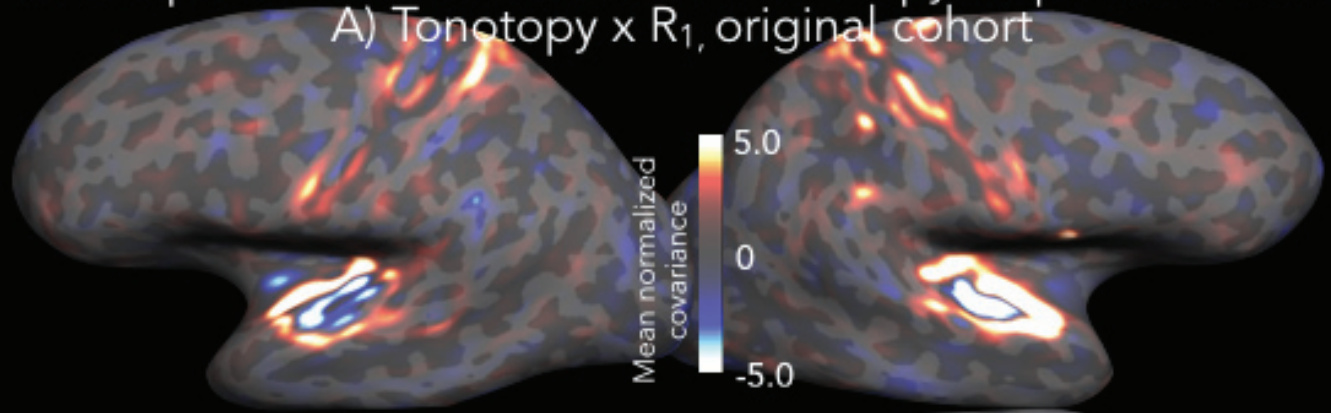




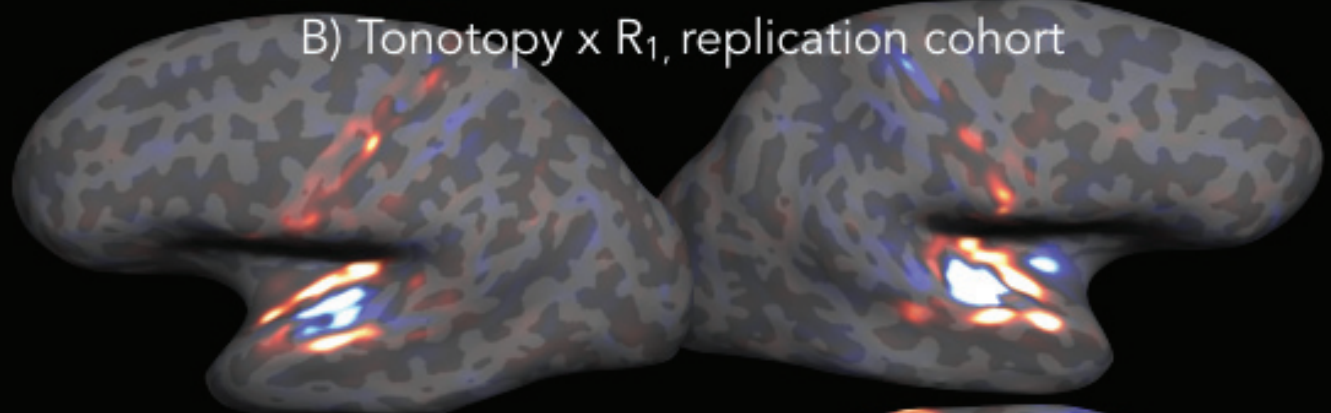


Local spatial covariance between tonotopy amplitude and  $R_1$

A) Tonotopy x  $R_1$ , original cohort



B) Tonotopy x  $R_1$ , replication cohort



C) Attn-o-topy x  $R_1$ , original cohort

